RESEARCH ARTICLE

Combinatorial ETS1-Dependent Control of Oncogenic NOTCH1 Enhancers in T-cell Leukemia

Anna C. McCarter[1], Giusy Della Gatta[2], Ashley Melnick[1], Erin Kim[3], Cher Sha[3], Qing Wang[3], Jahnavi K. Nalamolu[3], Yiran Liu[4], Theresa M. Keeley[5], Ran Yan[6], Mengxi Sun[7], Rohan Kodgule[8], Nicholas Kunnath[9], Alberto Ambesi-Impiombato[2], Rork Kuick[10,†], Arvind Rao[9], Russell J.H. Ryan[8], Barbara L. Kee[7], Linda C. Samuelson[1,5], Michael C. Ostrowski[11], Adolfo A. Ferrando[2,12,13,14], and Mark Y. Chiang[1,3]

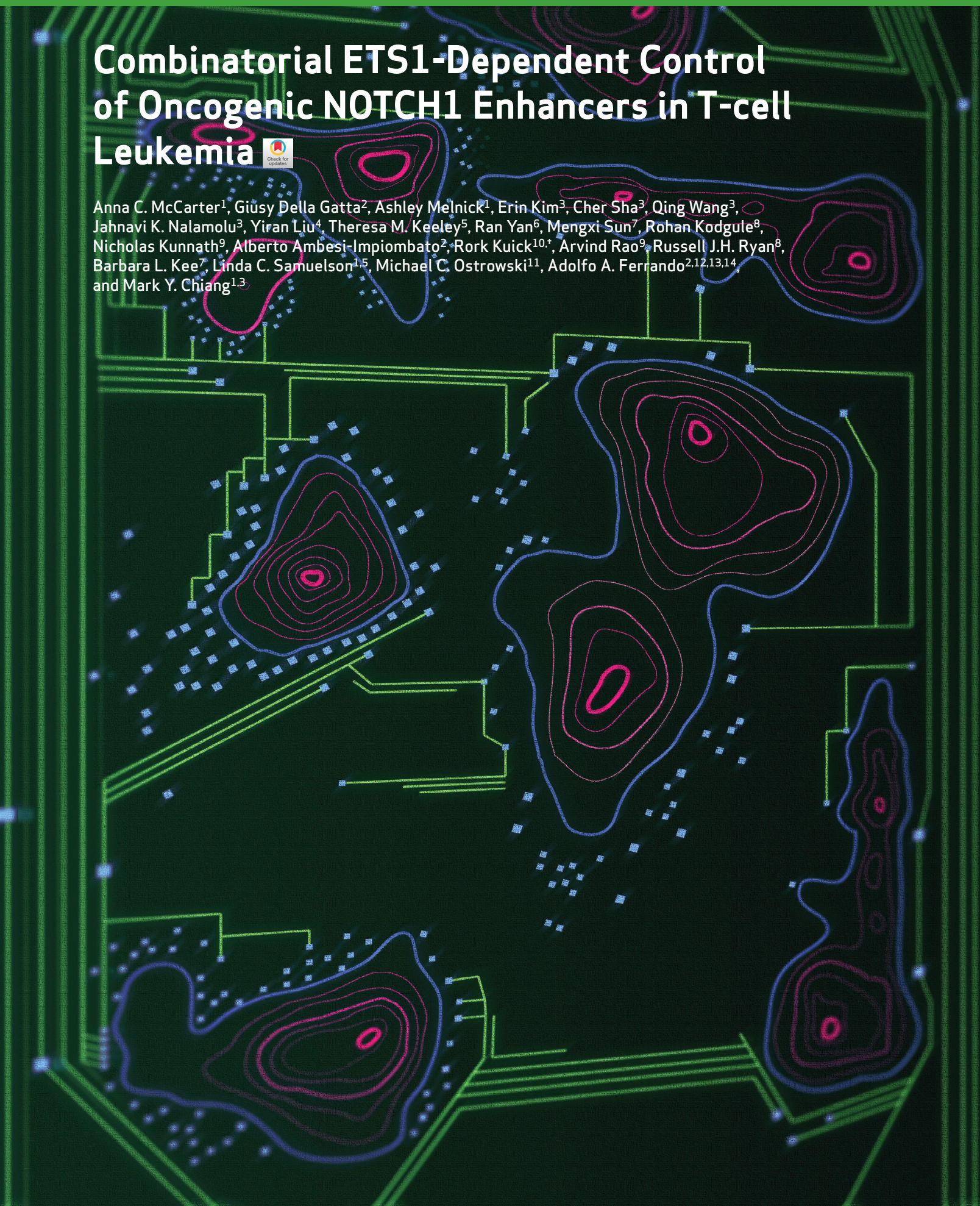

ABSTRACT Notch activation is highly prevalent among cancers, in particular T-cell acute lymphoblastic leukemia (T-ALL). However, the use of pan-Notch inhibitors to treat cancers has been hampered by adverse effects, particularly intestinal toxicities. To circumvent this barrier in T-ALL, we aimed to inhibit ETS1, a developmentally important T-cell transcription factor previously shown to cobind Notch response elements. Using complementary genetic approaches in mouse models, we show that ablation of Ets1 leads to strong Notch-mediated suppressive effects on T-cell development and leukemogenesis but milder intestinal effects than pan-Notch inhibitors. Mechanistically, genome-wide chromatin profiling studies demonstrate that Ets1 inactivation impairs recruitment of multiple Notch-associated factors and Notch-dependent activation of transcriptional elements controlling major Notch-driven oncogenic effector pathways. These results uncover previously unrecognized hierarchical heterogeneity of Notch-controlled genes and point to Ets1-mediated enucleation of Notch–Rbpj transcriptional complexes as a target for developing specific anti-Notch therapies in T-ALL that circumvent the barriers of pan-Notch inhibition.

SIGNIFICANCE: Notch signaling controls developmentally important and tissue-specific activities, raising barriers for developing anti-Notch therapies. Pivoting away from pan-Notch inhibitors, we show antileukemic but less toxic effects of targeting ETS1, a T-cell NOTCH1 cofactor. These results demonstrate the feasibility of context-dependent suppression of NOTCH1 programs for the treatment of T-ALL.

INTRODUCTION

The discovery of Notch-activated tumors, including approximately 60% of cases of T-cell acute lymphoblastic leukemia (T-ALL), spurred much interest and excitement to clinically test the efficacy and safety of pan-Notch inhibitors, such as gamma-secretase inhibitors (GSI), for the treatment of human cancers (1, 2). Notch receptors (Notch1–4) are activated by ligands in normal cells or additionally by activating mutations in cancer via cleavage by the gamma-secretase complex, which releases IntraCellular Notch (ICN). ICN translocates to the nucleus where it must interact with the DNA-binding Rbpj cofactor to induce transcription. Hence, small-molecule GSIs inhibit activation of Notch1–4 in normal and cancer cells. Unfortunately, early clinical trials in patients with cancer reported dose-limiting toxicities with continuous dosing of GSI (3–5). GSI toxicities result from abrogation of Notch signals crucial for normal homeostasis, particularly of the intestine (6–8), prompting the search for more specific ways to block Notch-induced oncogenic pathways. One idea to meet this challenge stems from *Drosophila* studies showing that cobinding of transcription factor partners at Notch response elements is necessary to generate cell-type–specific, Notch-driven gene expression programs (9). In vertebrates, Notch1 directly induces *MYC* expression in T-cell progenitors and T-ALL cells through the T-cell–specific Notch-*MYC* enhancer (N-ME; refs. 10, 11), which is selectively active and competent for Notch1-driven transcriptional activation through the pioneering activity of the chromatin remodeler GATA3 (12). Here, we hypothesized that Notch1-collaborating transcription factors are required to drive gene expression programs that promote Notch-induced T-ALL but less so to maintain tissue homeostasis. Inhibiting these factors could effectively oppose Notch signals in cancer while circumventing the toxicities of systemic pan-Notch inhibition with GSIs.

Ets1, the founding member of the Ets family of transcription factors, has biological functions and *in vivo* DNA-binding specificity that are distinct from other Ets proteins (13, 14). Ets1 has been proposed as a Notch1 coregulator as Ets1

[1]Cell and Molecular Biology Program, University of Michigan, Ann Arbor, Michigan. [2]Institute for Cancer Genetics, Columbia University, New York, New York. [3]Division of Hematology-Oncology, Department of Internal Medicine, University of Michigan, Ann Arbor, Michigan. [4]Stanford University, Stanford, California. [5]Department of Molecular and Integrative Physiology, University of Michigan, Ann Arbor, Michigan. [6]Cold Spring Harbor Laboratory, Cold Spring Harbor, New York. [7]Department of Pathology, University of Chicago, Chicago, Illinois. [8]Department of Pathology, University of Michigan, Ann Arbor, Michigan. [9]Department of Computational Medicine and Bioinformatics, University of Michigan, Ann Arbor, Michigan. [10]Department of Biostatistics, University of Michigan, Ann Arbor, Michigan. [11]Medical University of South Carolina, Charleston, South Carolina. [12]Department of Pathology and Cell Biology, Columbia University Medical Center, New York, New York. [13]Department of Pediatrics, Columbia University Medical Center, New York, New York. [14]Department of Systems Biology, Columbia University, New York, New York.

Note: Supplementary data for this article are available at Blood Cancer Discovery Online (http://bloodcancerdiscov.aacrjournals.org/).

A.C. McCarter and G. Della Gatta contributed equally to this article.

†Deceased.

Corresponding Authors: Adolfo A. Ferrando, Institute for Cancer Genetics, Columbia University Medical Center, 1130 Saint Nicholas Avenue, ICRC-402A, New York, NY 10032. Phone: 212-851-4611; E-mail: af2196@columbia.edu; and Mark Y. Chiang, University of Michigan, 109 Zina Pitcher Place, Room 2043 BSRB, Ann Arbor, MI 48109-2200. Phone: 734-615-7513; E-mail: markchia@med.umich.edu

Blood Cancer Discov 2020;1:178–97

doi: 10.1158/2643-3230.BCD-20-0026

binding at chromatin associates with Notch1 and Runx1 sites (15, 16), and like Notch1, Ets1 is required for T-cell development (17, 18). Consistently, Ets motifs are highly enriched in T-ALL–associated enhancers (19–22). These correlative observations are suggestive of a functional and clinically relevant interaction between Ets1 and Notch1 in early T-cell development and leukemogenesis. However, this concept should be formally tested, as other transcription factors involved in lymphoid development have shown to be dispensable for ALL leukemogenesis and in some cases, to actually work as tumor suppressors (23–27). Moreover, given that the scope of Ets1 expression, being primarily expressed in lymphoid cells (28), is more tissue-restricted than Notch during the postnatal period brings the possibility that a systemic Ets1 inhibitor could be less toxic than a GSI pan-Notch inhibitor. In this context, we proposed and experimentally tested the role of Ets1 as a Notch1-collaborating transcription factor in T-ALL. Our results formally establish a direct mechanistic role for Ets1 in the control of Notch1-dependent oncogenic programs in T-ALL and highlight Ets1 as a potential therapeutic target in this disease.

RESULTS

Ets1 Is Important for Notch-Dependent Steps of Early T-cell Development

A "Notch1-collaborating" transcription factor in T-ALL would be predicted to have overlapping functions with Notch1 in the normal thymic precursors from which T-ALL originates. Murine T-cell development proceeds in the thymus through a series of stages from the early T-lineage progenitor (ETP), through the double-negative (DN) stages (DN2–DN4) to the immature single-positive (ISP) and $CD4^+CD8^+$ double-positive (DP) stages, and then to the single-positive (SP) $CD4^+$ or $CD8^+$ stages. Notch1 is essential for two major stages of early T-cell development: ETP specification and the DN-to-DP transition (29). During thymocyte development, Ets1 and Notch target genes are concurrently expressed (Supplementary Fig. S1A). Ets1 is also expressed in the corresponding stages in human thymocytes (Supplementary Fig. S1B), which are susceptible to transformation to T-ALL (30). Thus, like Notch1, Ets1 is expressed in T-cell precursors that can transform into T-ALL.

The role of Ets1 during T-cell development was previously studied in germline *Ets1*-mutant mouse models. However, these early studies were hampered either because Ets1 function was partly intact (31) or because complete Ets1 deficiency was lethal to neonatal mice (32), which required studying thymopoiesis using Rag-deficient blastocyst complementation (17, 18). This precluded analysis of ETP specification, a critical Notch-dependent stage of T-cell development. Thus, to better study early thymopoiesis, we generated conditional *Ets1* knockout mice ($Ets1^{f/f}$). In this model, loxP sites flanked the DNA-binding Ets domain such that Cre-mediated recombination created an *Ets1*-null allele (17).

To delete *Ets1* in hematopoietic cells, we crossed $Ets1^{f/f}$ mice with *VavCre* mice generating *VavCre* $Ets1^{f/f}$ mice ($Ets1^{\Delta/\Delta}$). $Ets1^{\Delta/\Delta}$ mice showed >95% excision of the *Ets1* allele (Supplementary Fig. S1C) and undetectable Ets1 protein in the spleen (Supplementary Fig. S1D). Similar to Notch-deficient mice, $Ets1^{\Delta/\Delta}$ mice showed normal numbers of bone marrow $Lin^-Sca1^{hi}Kit^{hi}$ progenitors (LSK; Supplementary Fig. S1E and S1F) and lymphoid-primed multipotent progenitors (LMPP/MPP4; Supplementary Fig. S1G and S1H), which are the major extrathymic precursors of ETPs. In contrast, $Ets1^{\Delta/\Delta}$ mice showed profound depletion in total thymocyte number (~21-fold), which was more severe than seen in *VavCre* $Notch1^{f/f}$ mice (Fig. 1A and B). Like *VavCre* $Notch1^{f/f}$ mice (33), $Ets1^{\Delta/\Delta}$ mice showed defects in ETP specification (Fig. 1C and D) and loss of subsequent DN stages (Fig. 1C and E–K). These results support that, like Notch1, Ets1 is important for ETP specification in early T-cell development.

Notch1-deficient mice (34) show a defect in the DN-to-DP transition due to impaired TCRβ rearrangement and pre-TCR signaling (34). In contrast, $Ets1^{\Delta/\Delta}$ DN3 cells showed successful TCRβ rearrangement (Fig. 1C). Nevertheless, $Ets1^{\Delta/\Delta}$ cells were hampered in the DN-to-DP transition (Fig. 1L–N) and in their progression to the DN3b stage of development (Fig. 1O). This data is in agreement with defective pre-TCR signaling, as previously suggested in germline *Ets1*-null thymocytes (32). Consistent with the loss of the early T-cell subsets, subsequent T-cell stages in the thymus (Fig. 1L and P–S) and spleen (Supplementary Fig. S1I–S1K) were suppressed in $Ets1^{\Delta/\Delta}$ mice. Thus, Ets1 has overlapping roles with Notch1 in promoting pre-TCR signaling and the DN-to-DP transition.

As in the case of Notch1-deficient mice, Ets1-deficient animals did not show any general defects in B-cell numbers (Supplementary Fig. S1L and S1M). Moreover, we observed a mild myeloproliferative phenotype in Ets1-deficient mice (Supplementary Fig. S1N–S1P) that was reminiscent of that observed in Notch1/Notch2-deficient and Notch signaling–defective Nicastrin-deficient mice.

Ets1 Is Important for Notch-Induced T-ALL Maintenance

Next, we wondered whether the Ets1 dependence of T-cell precursors would be conserved after they transform to leukemia. To test this possibility, we used a well-established murine model of Notch-induced T-ALL (35, 36). We transduced bone marrow stem and progenitor cells of *Rosa26CreER*^{T2}, *Rosa26CreER*^{T2} $Ets1^{f/+}$, or *Rosa26CreER*^{T2} $Ets1^{f/f}$ mice with an activated *Notch1* allele (Δ*E/Notch1*; refs. 37, 38). We transplanted these cells into recipient mice to generate primary tumors (Fig. 2A; Supplementary Fig. S2A). To test the effect of *Ets1* deletion on T-ALL maintenance, we transferred primary tumors into secondary recipients, which were then injected with tamoxifen to induce *Ets1* deletion. In this setting, homozygous deletion of *Ets1* alleles caused approximately 32-fold loss of circulating leukemic cells and prolonged median survival by >100% compared with vehicle treatment controls (Fig. 2B–D). In contrast, heterozygous *Ets1* deletion had no effect on tumor progression and survival. We confirmed the survival benefit of homozygous *Ets1* deletion compared with control/heterozygous deletion with additional independent *Rosa26CreER*^{T2} (Supplementary Fig. S2B), *Rosa26CreER*^{T2} $Ets1^{f/+}$ (Supplementary Fig. S2C), and *Rosa26CreER*^{T2} $Ets1^{f/f}$ (Supplementary Fig. S2D) tumors. In these experiments, Cre activation induced mild or negligible effects in survival of control $Ets1^{+/+}$ or $Ets1^{f/+}$ T-ALL mice. In contrast, tamoxifen treatment conferred a marked and

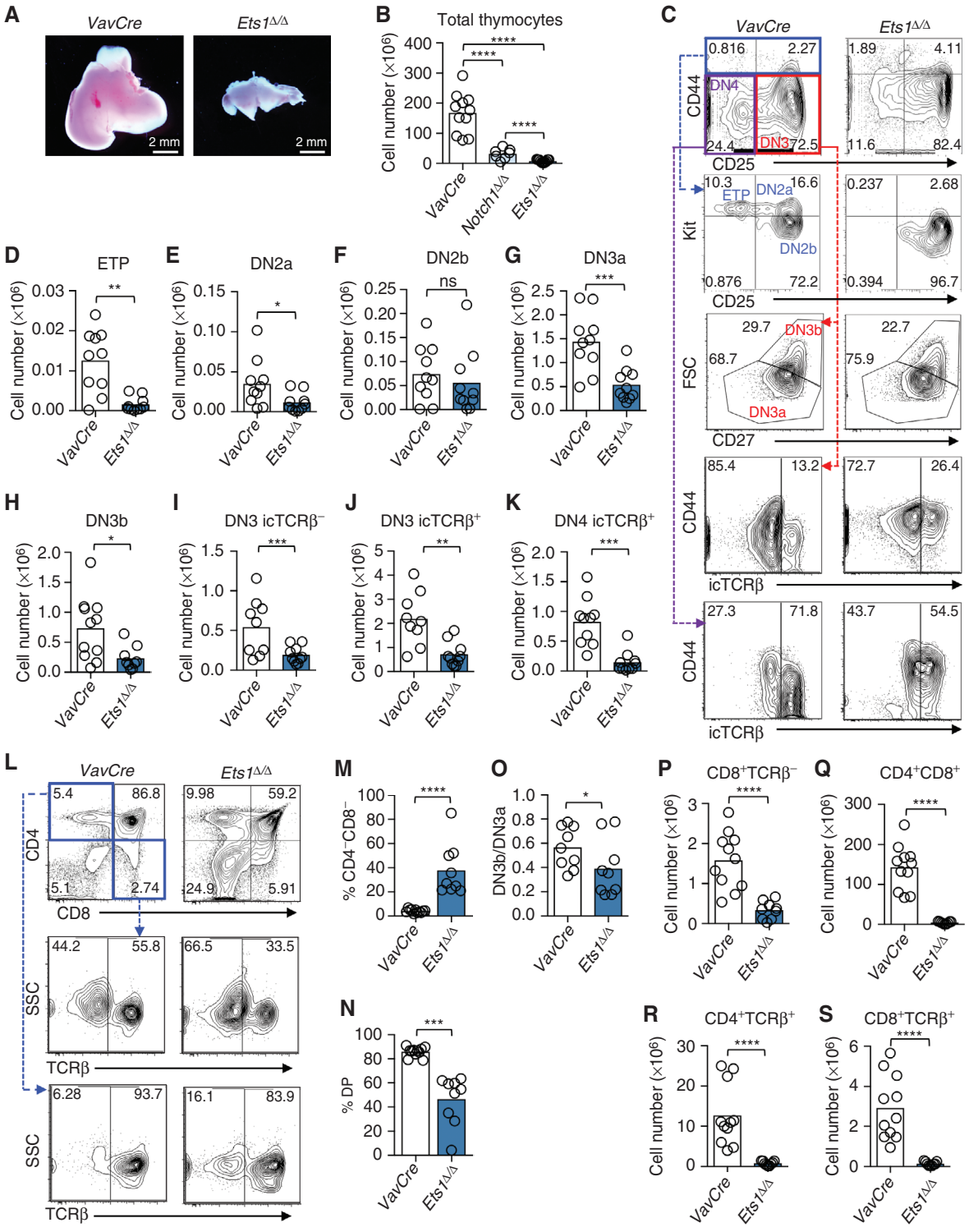

Figure 1. Ets1 is important for Notch-dependent steps of early T-cell development. **A,** Representative images of thymuses of *VavCre* control and *Ets1*$^{\Delta/\Delta}$ mice. **B,** Absolute numbers of total thymocytes in *VavCre* control, *Notch1*$^{\Delta/\Delta}$, and *Ets1*$^{\Delta/\Delta}$ mice. Representative flow cytometric profiles of DN subsets (**C**) and absolute numbers of ETP (**D**), DN2a (**E**), DN2b (**F**), DN3a (**G**), DN3b (**H**), DN3 icTCRβ$^-$ (**I**), DN3 icTCRβ$^+$ (**J**), and DN4 (**K**) subsets in *VavCre* control and *Ets1*$^{\Delta/\Delta}$ mice. Representative flow cytometry profiles of CD4/CD8 thymic subsets (**L**); %DN (**M**); %DP (**N**); DN3b/DN3a ratio (**O**); and absolute numbers of ISP (**P**), DP (**Q**), CD4 SP (**R**), and CD8 SP (**S**) thymic subsets in *VavCre* control and *Ets1*$^{\Delta/\Delta}$ mice. ns, not significant; *, $P < 0.05$; **, $P < 0.01$; ***, $P < 0.001$; ****, $P < 0.0001$. Two-sided two-sample *t* tests of nontransformed data were used for **M–O**. CD4 SP, CD4$^+$TCRβ$^+$; CD8 SP, CD8$^+$TCRβ$^+$; DN2a, Lineage$^-$CD44$^+$CD25$^+$cKit^{hi}; DN2b, Lineage$^-$CD44$^+$CD25$^+$cKit^{lo}; DN3, Lineage$^-$CD44$^-$CD25$^+$; DN3a, Lineage$^-$CD44$^-$CD25$^+$FSC^{lo}CD27$^-$; DN3b, Lineage$^-$CD44$^-$CD25$^+$FSC^{hi}CD27$^+$; DN4, Lineage$^-$CD44$^-$CD25$^-$; DP, CD4$^+$CD8$^+$; ETP, Lineage$^-$CD44$^+$CD25$^-$cKit^{hi}; ISP, CD8$^+$TCRβ$^-$.

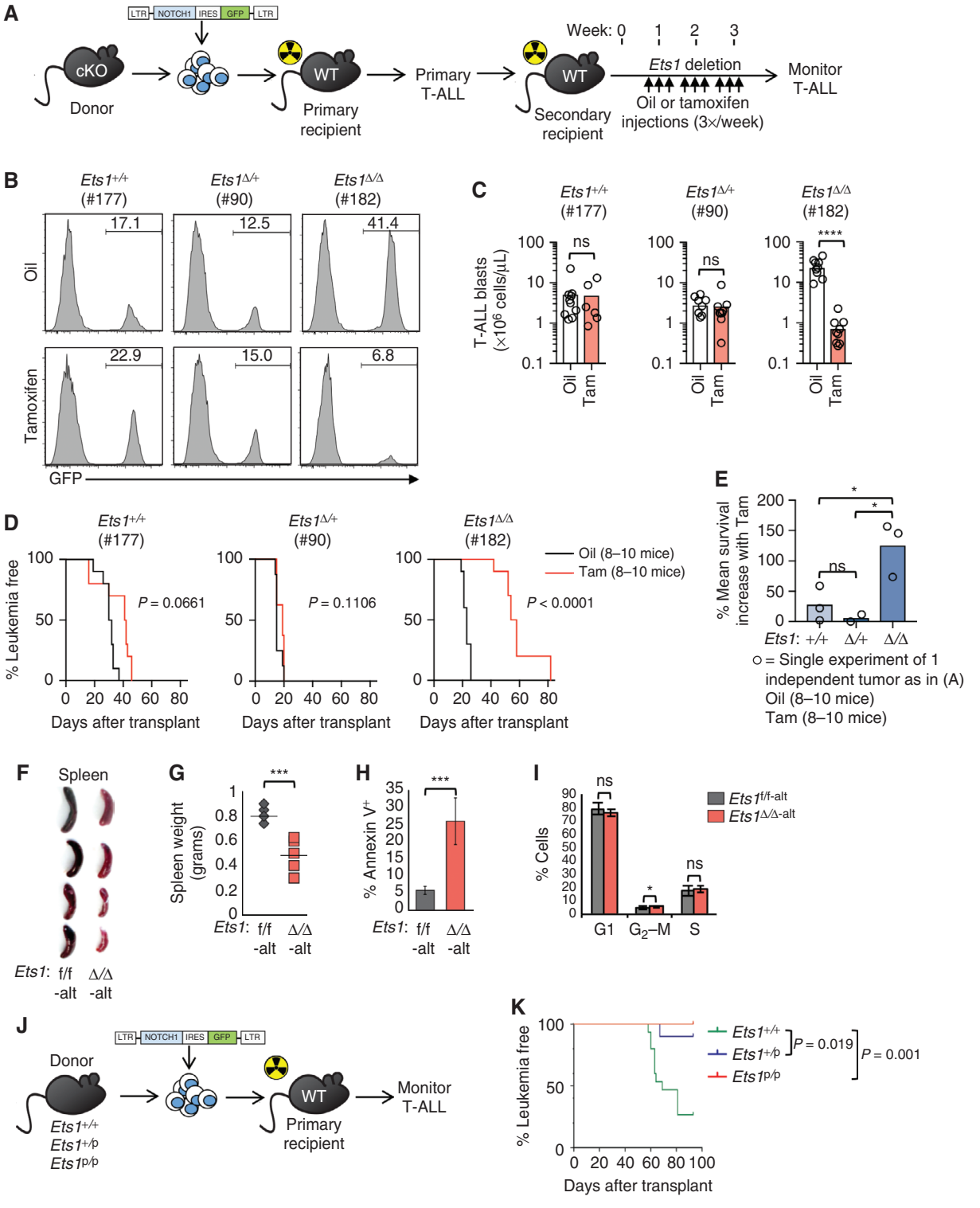

Figure 2. Ets1 is important for the maintenance and initiation of murine Notch-induced T-ALL. **A–E,** Experimental strategy to study maintenance of murine ΔE/Notch1-induced T-ALL (**A**). Tam, 25 mg/kg tamoxifen. Representative flow cytometric plots (**B**) and peripheral blood GFP+ T-ALL cell counts (**C**) at 2.5 weeks posttransplant, and survival curves (**D**) of mice transplanted with *Rosa26CreER*^{T2}, *Rosa26CreER*^{T2} *Ets1*$^{f/+}$, or *Rosa26CreER*^{T2} *Ets1*$^{f/f}$ T-ALL tumors. Tumor ID# shown in parentheses. **E,** Mean %survival increase comparing median survivals after tamoxifen versus vehicle injection of secondary recipient mice that were transplanted with two to three independent *Ets1*$^{+/+}$, *Ets1*$^{f/+}$, or *Ets1*$^{f/f}$ tumors. Images (**F**), weights (**G**), Annexin V analysis (**H**), and cell-cycle analysis (**I**) of splenic tumors from an alternative ("alt") Notch-induced T-ALL mouse model that were generated using the same experimental strategy (**A**) but were harvested from secondary recipients at 48 hours after injection with 300 mg/kg tamoxifen. **J–K,** Experimental strategy to study initiation of murine ΔE/Notch1-induced T-ALL (**J**). **K,** Survival curves of mice transplanted with *Ets1*$^{+/+}$, *Ets1*$^{p/+}$, or *Ets1*$^{p/p}$ bone marrow progenitors transduced with ΔE/Notch1 (ns, not significant; *, $P < 0.05$; **, $P < 0.01$; ***, $P < 0.001$; ****, $P < 0.0001$).

significant survival benefit of approximately 125% compared with vehicle treatment in the *Ets1*$^{f/f}$ T-ALL group (Fig. 2E).

The robust growth of *Ets1*$^{\Delta/+}$ tumors suggested that T-ALLs can thrive with only a single *Ets1* allele. Accordingly, the deletion efficiency of secondary splenic *Ets1*$^{\Delta/\Delta}$ tumors from morbid mice was only approximately 50%, which matched the approximately 50% deletion efficiency of *Ets1*$^{\Delta/+}$ tumors (Supplementary Fig. S2E). To investigate this further, we transplanted secondary *Ets1*$^{\Delta/\Delta}$ tumors into tertiary recipients. The deletion efficiency of tertiary tumors extracted from terminally diseased mice was also approximately 50% (Supplementary Fig. S2F). Collectively, in these experiments and our other experiences breeding floxed Ets1 mice, we did not observe preferential Cre-mediated deletion of the maternal or paternal *Ets1* allele. These results suggest that partial recombination resulting in deletion of only one *Ets1* allele is sufficient to support leukemia cell growth and drive genetic escape.

To further test the requirement of Ets1 in Notch-induced T-ALL maintenance, we acutely deleted *Ets1* in T-ALLs generated with a second conditional Ets1-deficient mouse model (39) and a different *Rosa26CreER*^{T2} strain with high deletion efficiency (40). To avoid confusion with the previous mouse model, we have labeled these mice as "*Ets1*$^{f/f\text{-}alt}$" and "*Rosa26CreER*$^{T2\text{-}alt}$," respectively. We deleted *Ets1* when GFP^{+} *Rosa26CreER*$^{T2\text{-}alt}$ *Ets1*$^{f/f\text{-}alt}$ T-ALL blasts comprised 50% to 60% of circulating white blood cells in secondary recipients using a dose of tamoxifen that does not induce toxicity in *Rosa26CreER*$^{T2\text{-}alt}$ control tumors (10, 41) and then harvested splenic tumors 48 hours later. Compared with controls, deletion of *Ets1* in *Ets1*$^{\Delta/\Delta\text{-}alt}$ tumors reduced spleen size (Fig. 2F and G) and increased apoptosis in T-ALL blasts (Fig. 2H) with modest effects on cell cycle (Fig. 2I). In all, complementary experiments using two independently derived genetic mouse models show that Ets1 is important for maintenance of Notch-induced T-ALL.

Ets1 Is Important for Initiation of Notch-Induced T-ALL

To determine the effect of *Ets1* deletion on initiation of Notch-induced T-ALL, we used a previously described "*Ets1*$^{p/p}$" mouse, which produces a hypomorphic Ets1 protein lacking the N-terminal PNT domain (31). These mice show a weak Ets1 loss-of-function phenotype with an approximately 2.8-fold loss of thymocytes (42). We transduced bone marrow stem and progenitor cells from *Ets1*$^{+/+}$, *Ets1*$^{+/p}$, or *Ets1*$^{p/p}$ mice with ΔE/Notch1 and transplanted these into isogenic recipient mice (Fig. 2J). Most mice injected with *Ets1*$^{+/+}$ cells died of leukemia 90 days after transplant. In contrast, 6% and 0% of mice transplanted with *Ets1*$^{+/p}$ and *Ets1*$^{p/p}$ cells, respectively, died of T-ALL (Fig. 2K). These data demonstrate a strict requirement of Ets1 function for *in vivo* initiation of Notch-induced T-ALL.

ETS1 Is Important for Propagation of Human T-ALL Cells

ETS1 was one of the most highly and consistently expressed Ets transcription factor genes in primary human T-ALL samples (Fig. 3A) and patient-derived xenografts (PDX; Supplementary Fig. S3A). In a clinically annotated cohort of pediatric T-ALL, high *ETS1* expression was associated with hyperleukocytosis (white blood cell count >100K; Supplementary Fig. S3B), but not survival (Supplementary Fig. S3C). To test the functional importance of ETS1 in human T-ALL, we transduced *ETS1* shRNAs into T-ALL cell lines. In-depth analysis of ETS1 knockdown in HPB-ALL cells showed effective suppression of ETS1 protein and mRNA levels (Supplementary Fig. S3D and S3E), reduced proliferation (Supplementary Fig. S3F), and delayed G_1–S transition (Supplementary Fig. S3G). Similarly, ETS1 knockdown reduced proliferation of six of eight additional cell lines tested (CEM, THP-6, DND-41, SUP-T1, MOLT4, and DU.528; Fig. 3B–E; Supplementary Fig. S3H–S3M).

To test the antitumor effects of *ETS1* inactivation in non-immortalized human T-ALL cells *in vivo*, we took advantage of the success of shRNA protocols in knocking down gene expression in PDX cells. In these experiments, we transduced PDX3 cells, which expressed high levels of ETS1 and NOTCH1 (Fig. 3F) with shETS1/YFP and transplanted them into immunodeficient NSG mice (Fig. 3G). Knockdown cells were viable, as they could expand for several more days *in vitro* (Fig. 3H and I). However, ETS1 inactivation markedly blunted disease progression, reducing circulating T-ALL blasts by 44-fold at 8 weeks posttransplant (Fig. 3J and K), and improved survival (Fig. 3L). Moreover, PDX cells that were recovered from terminally diseased mice showed reduced levels of YFP (Fig. 3M) and restored *ETS1* expression (Fig. 3N), consistent with positive selection of cells that escaped ETS1 knockdown. Taken together, these results demonstrate a strong and highly prevalent ETS1-dependency in human T-ALL.

Ets1 Deficiency Is Less Toxic than the Pan-Notch Inhibitor GSI

Next, we explored the effects of *Ets1* inactivation on overall health and, in particular, the intestine, which is the major organ affected by the toxicity of GSI in humans and mice (8, 43). We induced ubiquitous *Ets1* deletion in *Rosa26CreER*^{T2} *Ets1*$^{f/f}$ mice via tamoxifen injection. In these experiments, *Ets1*ΔRosa26CreER^{T2} mice showed 70% to 90% *Ets1* deletion (Fig. 4A) and undetectable Ets1 protein in the intestine (Fig. 4B). *Ets1*Δ*Rosa26CreER*^{T2} mice showed no significant differences in weight (Supplementary Fig. S4A) and survival compared with controls (Supplementary Fig. S4B). To characterize the effects of *Ets1* deletion, we analyzed *Ets1*Δ*Rosa26CreER*^{T2} mice after tamoxifen injection. At 24 days, *Ets1*-deleted mice showed unremarkable blood counts other than the expected lymphopenia (Supplementary Fig. S4C). Histologic analysis of Ets1-deficient spleens showed preserved white pulp cellularity and decreased myeloid component of the red pulp compared with control spleens (Supplementary Fig. S4D). Analysis of the intestinal tissues of *Ets1*Δ*Rosa26CreER*^{T2} mice showed morphologic changes that were similar but less pronounced than those observed in mice after pan-Notch inactivation with GSI (Fig. 4C–F). Specifically, *Ets1*Δ*Rosa26CreER*^{T2} mice showed modest reductions in duodenal villi length (Fig. 4G), a trend toward increased duodenal crypt depth (Fig. 4H), and modest ileal goblet cell metaplasia (Fig. 4I). Similar but more pronounced changes were observed in GSI-treated

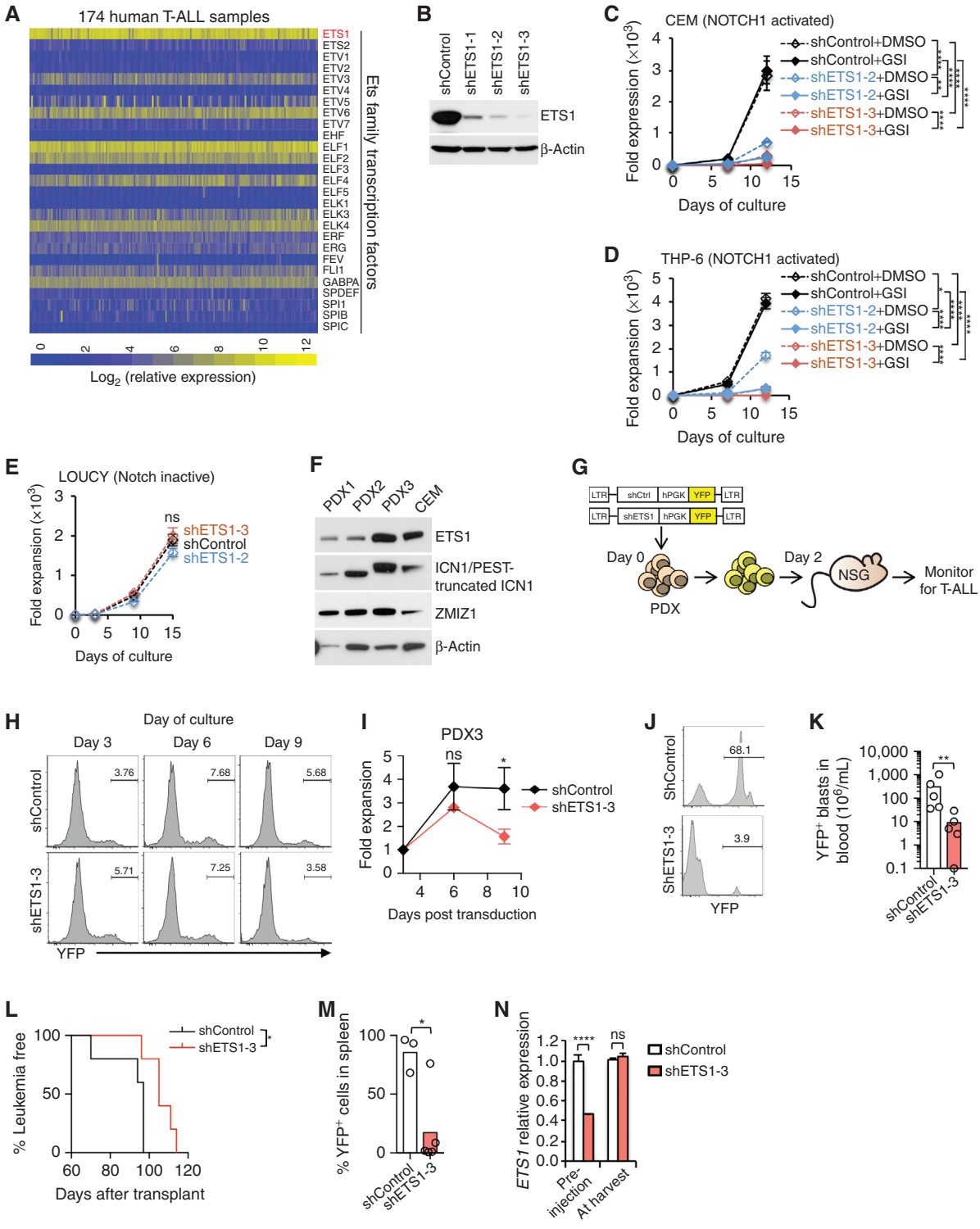

Figure 3. ETS1 is important for propagation of human T-ALL cells. **A,** Heatmap of Ets family member mRNA in primary human T-ALL samples (GSE13159). **B,** Western blot analysis of ETS1 in CEM cells transduced with shETS1. Growth curves of CEM (**C**), THP-6 (**D**), and LOUCY (**E**) T-ALL cells transduced with shETS1. GSI, 200 nmol/L DBZ. Fold expansion = cell count divided by cell count on day 0. **F,** Western blot analysis of ETS1, cleaved NOTCH1 (ICN1), and ZMIZ1 in PDX samples. **G–N,** Experimental strategy testing maintenance of PDX cells transduced with shETS1-3/YFP after transplantation into NSG mice (**G**). Flow cytometric plots (**H**) and growth curves (**I**) of PDX cells transduced on day 0, sorted on day 2, and cocultured with OP9-DLL4 cells. $N = 3$ transduced bioreplicates per group. Representative flow cytometric plots (**J**) and peripheral blood T-ALL counts (**K**) at 8 weeks posttransplant; survival curves (**L**); and %YFP (**M**) and *ETS1* transcripts normalized to respective controls (**N**) of splenic tumors harvested from terminally diseased mice (99.3% hCD45-positive T-ALL content) compared with cells prior to injection into NSG mice (ns, not significant; *, $P < 0.05$; **, $P < 0.01$; ****, $P < 0.0001$).

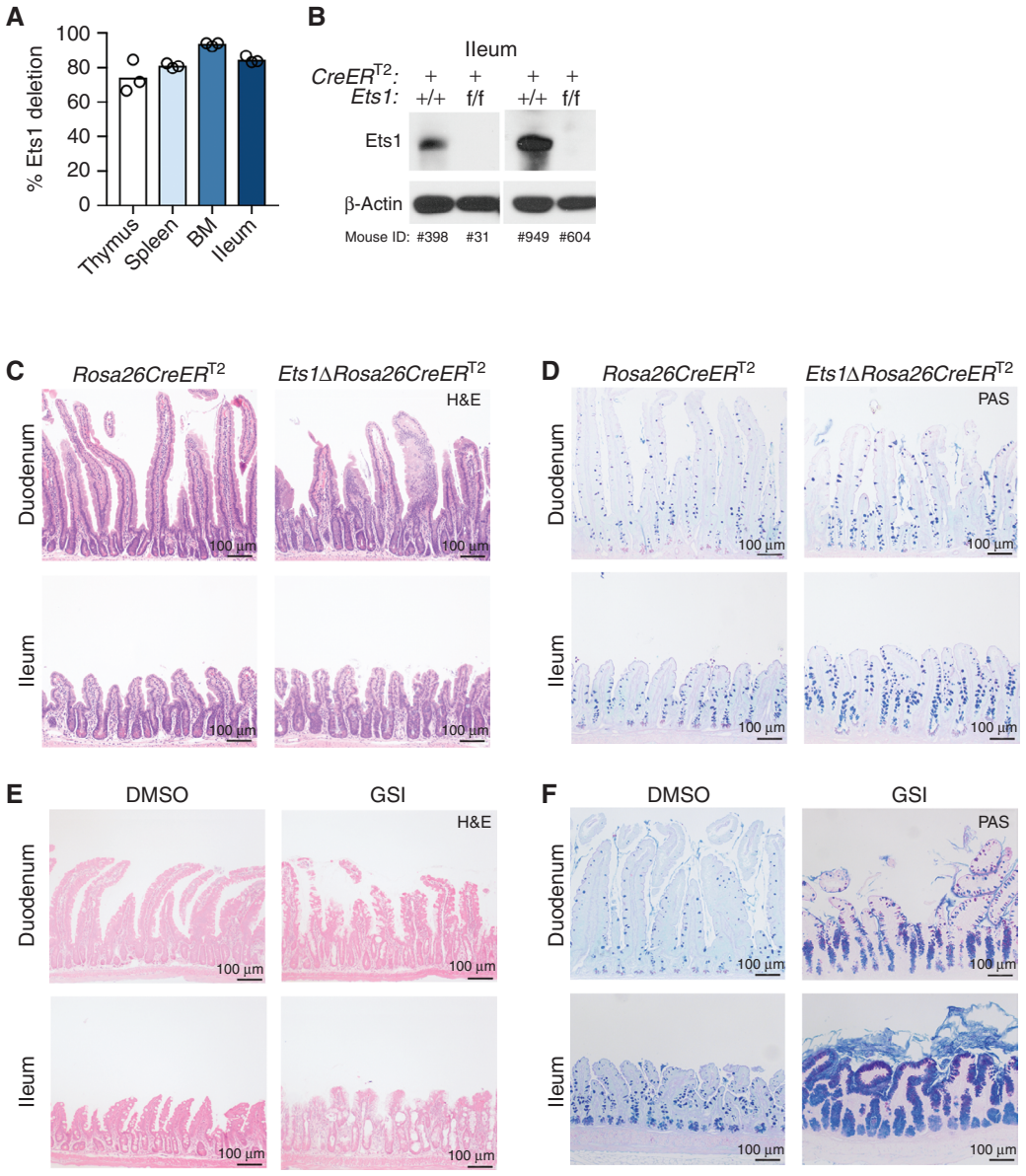

Figure 4. Ets1 deficiency is less toxic than the pan-Notch inhibitor GSI. **A,** qPCR showing *Ets1* deletion efficiency in thymus, spleen, bone marrow (BM), and intestine DNA of *Ets1ΔRosa26CreER*^{T2} mice after three doses of 150 mg/kg tamoxifen. **B,** Western blot analysis for Ets1 in *Rosa26CreER*^{T2} control and *Ets1ΔRosa26CreER*^{T2} intestine after the third dose of tamoxifen. Representative hematoxylin and eosin (H&E) (**C**) and PAS/AB (**D**) images of duodenum and ileum from *Rosa26CreER*^{T2} control and *Ets1ΔRosa26CreER*^{T2} mice harvested 8 days after the third dose of tamoxifen. Representative H&E (**E**) and PAS/AB (**F**) images of duodenum and ileum harvested from mice 1 day after 5 consecutive days of injection with DMSO or 30 μmol/kg GSI (DBZ). (*continued on next page*)

mice (Fig. 4J–L). Furthermore, we generated mice with intestinal-specific deletion using the *VillinCreER*^{T2} transgene. *Ets1ΔVillinCreER*^{T2} mice showed 80% to 90% *Ets1* deletion in intestinal crypt cells (Supplementary Fig. S4E). In contrast to *Notch1ΔVillinCreER*^{T2} mice (7), we did not observe any changes in villus morphology, goblet cell abundance, or weight (Supplementary Fig. S4F–S4K). These data suggest that systemic Ets1 inhibition only partially recapitulates the phenotype of systemic Notch inhibition with GSIs and induces limited toxicity.

ETS1 Promotes NOTCH1-Driven Oncogenic Pathways

We next sought to understand the underlying mechanism of the Ets1 requirement for Notch1-induced T-ALL initiation and maintenance. Toward this goal, we performed RNA sequencing (RNA-seq) in THP-6 T-ALL cells following ETS1 knockdown and NOTCH1 inhibition using GSI. These analyses revealed broadly overlapping signatures between ETS1 and NOTCH1 deprivation. About 33% of ETS1-regulated genes

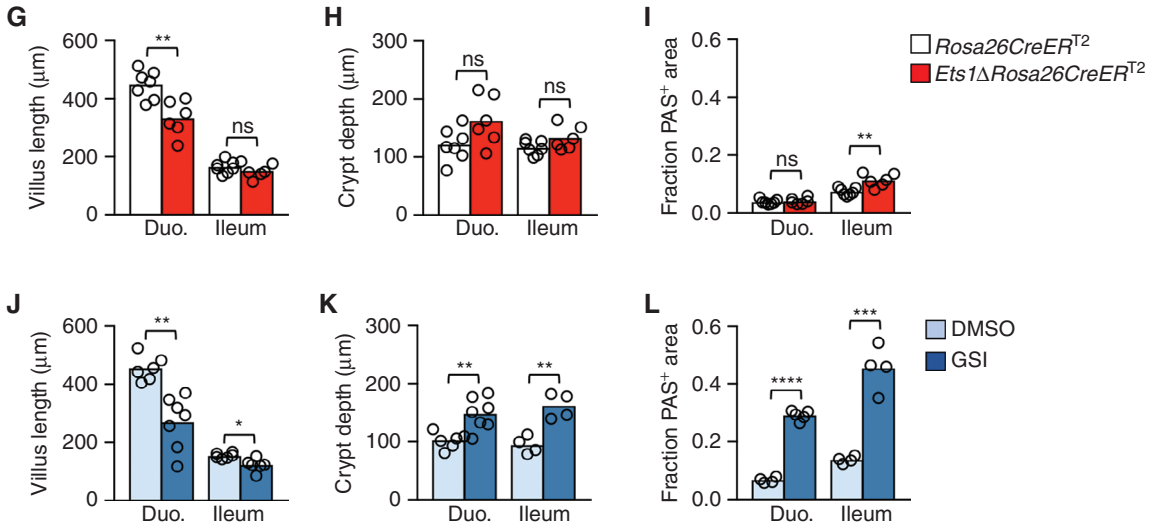

Figure 4. ***(Continued)*** Quantitation of villus length (**G** and **J**), crypt depth (**H** and **K**), and fraction of PAS$^+$ area (**I** and **L**) from *Rosa26CreER*^{T2} control and *Ets1ΔRosa26CreER*^{T2} mice after the third dose of tamoxifen (**G–I**) or 5 days after 5 consecutive days of injection with DMSO/GSI (**J–L**; ns, not significant; *, $P < 0.05$; **, $P < 0.01$; ***, $P < 0.001$; ****, $P < 0.0001$). Duo., duodenum.

were also controlled by NOTCH1 (Fig. 5A). Conversely, about 22% of NOTCH1-controlled genes were also regulated by ETS1. Of the 467 ETS1-NOTCH1 coregulated genes, 290 (62%) were regulated in the same direction. Interestingly, pathway analyses showed Myc target genes as the most prominent Hallmark signature enriched in ETS1-induced and NOTCH1-induced genes (ETS1 NES = −5.81, FDR < 0.0001; NOTCH1 NES −6.15, FDR < 0.0001; Fig. 5B and C; Supplementary Table S1). Consistently, pathway analyses showed that the list of genes containing at least one Myc binding motif (CACGTG) and the C6 oncogenic signature of Myc-induced genes were among the topmost enriched in ETS1-induced and NOTCH1-induced genes (FDR < 0.0001; Supplementary Table S1; Supplementary Fig. S5A and S5B). In addition, pathway analyses showed that the C6 oncogenic signature of mTOR-induced genes and the mTOR-related Rapamycin_Response and Leucine_Deprivation gene sets were highly enriched in ETS1-induced and NOTCH1-induced genes (FDR < 0.01; Supplementary Table S1; Supplementary Fig. S5A and S5B). These results reinforce the well-established roles for Myc and mTOR as major oncogenic effector pathways in Notch1-induced T-ALL (2). To test the importance of MYC and mTOR as downstream effectors of the ETS1-driven oncogenic/dependency programs, we expressed Myc or myr-AKT in THP-6 cells (Supplementary Fig. S5C) and CEM cells (Supplementary Fig. S5D) using previously described constructs (44). Enforced expression of Myc or myr-AKT was sufficient for partial rescue from the antiproliferative effects of ETS1 deprivation. These data support the prominent role of MYC and mTOR signaling in ETS1 programs convergent with NOTCH1 in the control of T-ALL proliferation. Moreover, it did not escape our attention that several known direct NOTCH1 target genes were downregulated by ETS1 knockdown, including *MYC, NOTCH3, HES1, DTX1, SHQ1, NOTCH1*, and *IL7R* (Q < 0.05; Fig. 5D; Supplementary Fig. S5E–S5G; Supplementary Table S2).

Similarly, ETS1-regulated genes in HPB-ALL cells (Supplementary Table S3) were significantly enriched in a core set of NOTCH1-regulated genes shared among seven T-ALL cell lines (ref. 45; $P < 0.001$; Fig. 5E). Moreover, corner gene analysis showed markedly concordant effects of ETS1

Figure 5. ETS1 promotes Notch-driven oncogenic pathways in T-ALL. **A,** Venn diagram showing ETS1 and NOTCH1 target genes in THP-6 cells. ETS1 target genes = $P < 0.01$ and fold change (FC) > 1.2 for the comparison of shControl versus both shETS1 (3/2). NOTCH1 target genes = $P < 0.01$ and FC > 1.2 for the DMSO versus GSI comparison. Gene set enrichment analysis (GSEA) using the MSigDB HALLMARK_MYC_V2 list for the shControl versus shETS1-3/2 (**B**) and DMSO versus GSI (**C**) comparisons. **D,** Volcano plot of RNA-seq Log_2FC data showing the shControl versus shETS1-3 comparison and selected NOTCH1 (yellow) and non-NOTCH1 (blue) target genes. GSEA using list of shared NOTCH1 target genes in T-ALL (45) for the shLUC versus shETS1-4 comparison in HPB-ALL cells (**E**), and heatmaps of the top 28 downregulated genes (red box in **E**) in HPB-ALL cells merged with the corresponding genes for the shControl versus shETS1-3/2 comparison and the DMSO versus GSI comparison in THP-6 cells (**F**). *P* values represent Mantel–Haenszel χ^2 tests of association of the indicated comparisons between HPB-ALL cells and THP-6 cells. **G,** Volcano plot of ETS1 ChIP-seq Log_2FC in THP-6 cells showing the shControl versus shETS1-3 comparison and target genes in **D** that are located within the same TAD (GSM3967126; ref. 65) as the ETS1 peaks. **H,** Violin plots showing the ETS1 ChIP-seq Log_2FC in THP-6 cells of all ETS1 peaks and dynamic ETS1 peaks. Number of peaks of each type are indicated. Dynamic ETS1 peaks = union intervals with $Log_2FC < 0$ and FDR < 0.1 for both shControl versus shETS1-3/2 comparisons. Red line = median. **I,** Violin plots showing the H3K27ac ChIP-seq Log_2FC at all ETS1 peaks, dynamic ETS1 peaks, and ETS1 peaks that cobind RBPJ peaks or ZMIZ1 peaks that decrease (FDR < 0.1) with both shETS1 (3/2). ETS1 and H3K27ac ChIP-seq tracks in THP-6 cells transduced with shETS1-3 at the TADs encompassing the *MYC* (**J**) and *MYB* (**K**) genomic loci. *ETS1-dependent enhancers = sites of dynamic ETS1 peaks where H3K27ac decreases with FDR < 0.1. "a" and "b" are biological replicates. CUTLL1 ChIP-seq (GSE51800; ref. 15), H3K27ac Hi-ChIP (GSM3967135; ref. 65), and Hi-C TAD (GSM3967126; ref. 65) datasets are shown. NES, normalized enrichment scale; w4h, 4 hours after GSI washout.

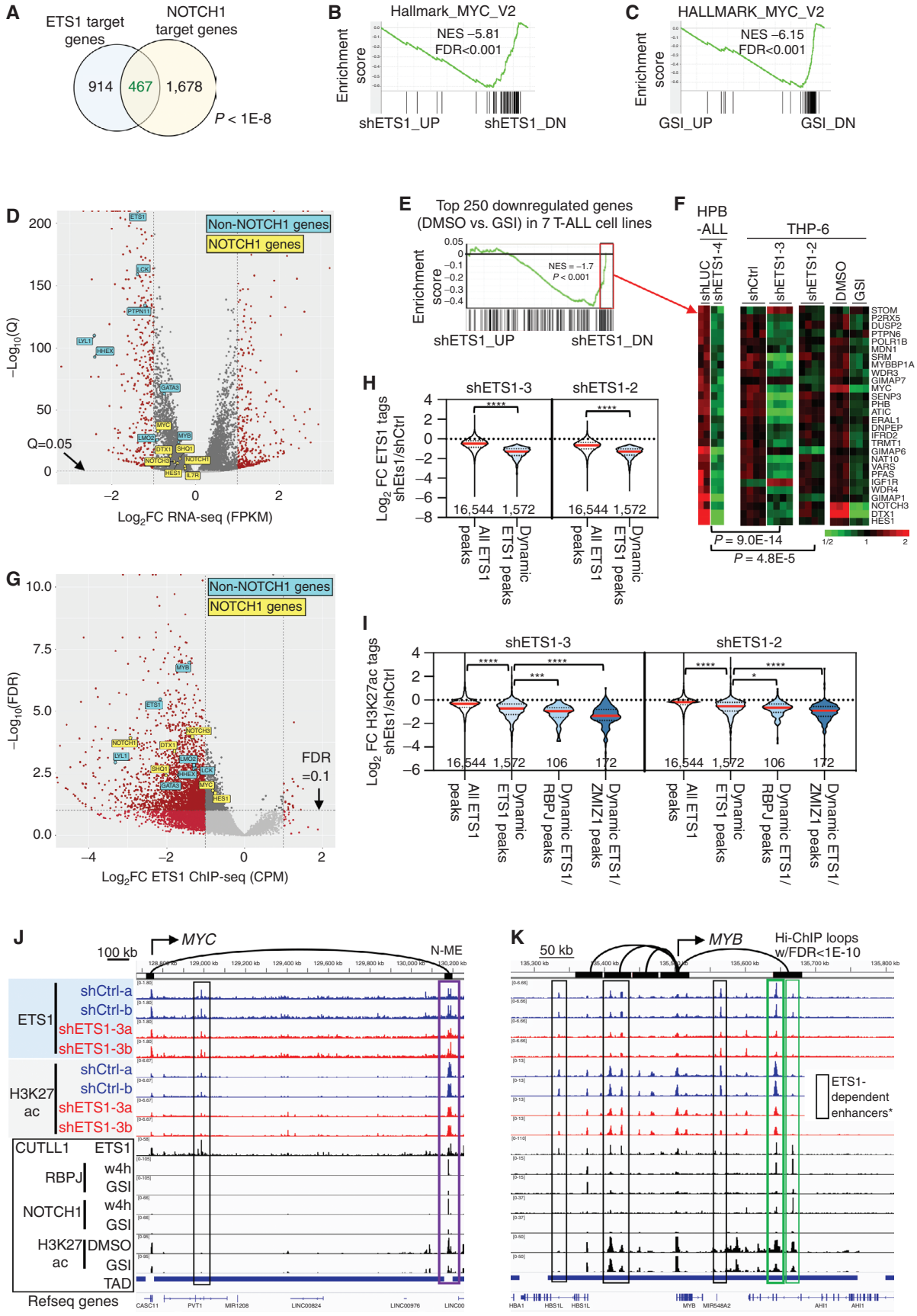
A
ETS1 target genes
NOTCH1 target genes
914
467
1,678
P < 1E-8
B
Hallmark_MYC_V2
NES –5.81
FDR<0.001
Enrichment score
shETS1_UP
shETS1_DN
C
HALLMARK_MYC_V2
NES –6.15
FDR<0.001
Enrichment score
GSI_UP
GSI_DN
D
Non-NOTCH1 genes
NOTCH1 genes
–Log10(Q)
Q=0.05
Log2FC RNA-seq (FPKM)
E
Top 250 downregulated genes
(DMSO vs. GSI) in 7 T-ALL cell lines
NES = –1.7
P < 0.001
Enrichment score
shETS1_UP
shETS1_DN
F
HPB -ALL
THP-6
shLUC
shETS1-4
shCtrl
shETS1-3
shETS1-2
DMSO
GSI
STOM
P2RX5
DUSP2
PTPN6
POLR1B
MDN1
SRM
MYBBP1A
WDR3
GIMAP7
MYC
SENP3
PHB
ATIC
ERAL1
DNPEP
IFRD2
TRMT1
GIMAP6
NAT10
VARS
PFAS
IGF1R
WDR4
GIMAP1
NOTCH3
DTX1
HES1
P = 9.0E-14
P = 4.8E-5
H
shETS1-3
shETS1-2
Log2 FC ETS1 tags shEts1/shCtrl
16,544
1,572
All ETS1 peaks
Dynamic ETS1 peaks
G
Non-NOTCH1 genes
NOTCH1 genes
–Log10(FDR)
FDR =0.1
Log2FC ETS1 ChIP-seq (CPM)
I
shETS1-3
shETS1-2
Log2 FC H3K27ac tags shEts1/shCtrl
16,544
1,572
106
172
All ETS1 peaks
Dynamic ETS1 peaks
Dynamic ETS1/ RBPJ peaks
Dynamic ETS1/ ZMIZ1 peaks
J
100 kb
MYC
N-ME
ETS1
shCtrl-a
shCtrl-b
shETS1-3a
shETS1-3b
H3K27 ac
CUTLL1
RBPJ
NOTCH1
w4h
GSI
DMSO
TAD
Refseq genes
K
50 kb
MYB
Hi-ChIP loops w/FDR<1E-10
ETS1-dependent enhancers*

deprivation between THP-6 and HPB-ALL (P = 1E-190; Supplementary Fig. S5I and S5J; Supplementary Table S2). Of the top 28 NOTCH1-controlled genes, most downregulated by shETS1-4 in HPB-ALL cells, 23 were also downregulated by shETS1-3 in THP-6 cells (P = 9.0E-14; Fig. 5F; Supplementary Table S2), including well-established NOTCH1-induced target genes like *MYC, DTX1, HES1*, and *NOTCH3* (Fig. 5D and F; Supplementary Fig. S5H). In all, the results show that ETS1 and NOTCH1 coinduce shared target genes and oncogenic pathways across multiple T-ALL cell lines.

Dynamic ETS1 Binding Increases H3K27ac at GATA-Associated Response Elements

We next asked, what are the direct effects of ETS1 on enhancer and transcriptional activation? To answer this question, we performed ETS1 chromatin immunoprecipitation sequencing (ChIP-seq) in THP-6 cells following ETS1 knockdown. We defined "dynamic ETS1 peaks" as those with differential ChIP-seq read count FDR < 0.1 for two independent ETS1 shRNA knockdowns compared with controls. Using these parameters, we identified 3,697 dynamic ETS1 peaks (Fig. 5G; Supplementary Fig. S5K) in which ETS1 knockdown significantly reduced ETS1 occupancies compared with all ETS1 binding sites (Fig. 5H). Only approximately 15% of ETS1 peaks met criteria as dynamic ETS1 peaks. Moreover, transcription factor motif analysis showed that 70% of dynamic ETS1 peaks contained the HOMER Ets1 motif compared with only 35% of nondynamic ETS1 peaks, indicating that dynamic ETS1 peaks could signify a class of high-confidence ETS1 binding sites. Next, we identified dynamic ETS1 peaks located within the same topologically associating domain (TAD) of 1,739 genes differentially expressed after ETS1 knockdown (DEG; Q < 0.05 for both shETS1) and designated these loci as "high-confidence direct ETS1 target genes" (Fig. 5G; Supplementary Fig. S5K; Supplementary Table S4). Among these, 1,011 genes showed chromatin looping linking promoter regulatory sequences with a distal dynamic ETS1 peak based on H3K27ac Hi-ChIP (Supplementary Table S4). Of these genes, 430 (43%) were also NOTCH1 target genes at Q < 0.05. These data suggest that ETS1 directly co-regulates a large fraction of the Notch transcriptional program.

To evaluate the functional role of ETS1 in enhancer regulation, we performed H3K27ac ChIP-seq in THP-6 cells in basal conditions and following ETS1 knockdown. In these experiments, ETS1 deprivation reduced H3K27ac read counts at dynamic ETS1 peaks compared to all ETS1 peaks (Fig. 5I). Mean Log_2FC differences were −0.479 and −0.412 for shETS1-3 and shETS1-2 compared with controls, respectively, in line with the known interaction of ETS1 with P300/CBP acetyl transferases. However, only approximately 51% of dynamic ETS1 peaks were associated with differential H3K27ac read counts. To better understand the regulatory logic by which ETS1 facilitates activation of response elements, we performed *de novo* HOMER motif analysis of dynamic ETS1 peaks associated with differential H3K27ac read counts following ETS1 knockdown (Supplementary Fig. S5L). These analyses recovered an Ets family motif as the top hit and a sequence closely matching GATA family motifs as the second most frequent element associated with dynamic ETS1 peaks linked to H3K27ac regulation compared with all other dynamic ETS1 peaks (26% vs. 16%; P = 1E-8). On the basis of these findings, we propose that ETS1 and GATA3 cooperate in promoting enhancer activation.

To better understand the impact of ETS1 control of oncogenic programs in T-ALL, we examined the effect of ETS1 deprivation on enhancers located in the same TADs containing *MYC* (Fig. 5J) and *MYB* (Fig. 5K), two major T-ALL oncogenes. H3K27ac Hi-ChIP data identified the N-ME (purple box, Fig. 5J) as the only enhancer associated with the *MYC* promoter in CUTLL1 cells at FDR < 1E-10. In contrast, multiple enhancers were associated with the *MYB* promoter (Fig. 5K). Two *MYB* enhancers showed dynamic NOTCH1/RBPJ binding associated with differential H3K27ac signals (Fig. 5K). In this context, ETS1 deprivation reduced ETS1 and H3K27ac read counts at the N-ME and multiple *MYB*-associated enhancers, including the Notch-bound *MYB* distal regulatory sites. Importantly, we observed convergent and largely overlapping ETS1 and H3K27ac peaks associated with *MYC* and *MYB* in THP-6 and CUTLL1 cells, supporting a common regulatory logic across T-ALL tumors. Overall, 72% of ETS1 peaks identified in THP-6 cells were detected in CUTLL1 cells (Supplementary Fig. S5M). Altogether, these results indicate a prominent role for ETS1 binding in the activation of enhancers driving oncogene expression in T-ALL.

ETS1 Interacts with NOTCH1 and Cooccupies Most ICN1/RBPJ Binding Sites

The convergent transcriptional effects of ETS1 and NOTCH1 in T-ALL led us to ask the question, does ETS1 interact closely with NOTCH1? To answer this question, we first tested whether ETS1 could physically bind the Notch transcriptional complex. Accordingly, coimmunoprecipitation experiments in THP-6 and HPB-ALL cells showed interactions between endogenous ETS1 and activated intracellular NOTCH1 proteins (Fig. 6A; Supplementary Fig. S6A). In

Figure 6. ETS1 facilitates recruitment of Notch complex members to response elements enriched for GATA factor binding motifs. **A,** Endogenous coimmunoprecipitation assays showing interactions between ETS1, cleaved NOTCH1 (ICN1), and ZMIZ1 in THP-6 cells. **B,** Venn diagram showing overlaps between ETS1, RBPJ, ICN1, and ZMIZ1 ChIP-seq peaks in control THP-6 cells. **C,** Top, violin plots showing the RBPJ ChIP-seq Log_2FC of all RBPJ peaks and RBPJ peaks that overlap with dynamic ETS1 peaks. Bottom, HOMER *de novo* motif analysis of RBPJ peaks that cobind dynamic ETS1 peaks and decrease upon ETS1 deprivation. The top five motifs with the lowest P values are shown with subsequent known motif analysis comparing RBPJ peaks overlapping with dynamic ETS1 peaks that decrease with FDR < 0.1 or do not decrease with FDR < 0.1 for two shETS1 (3/2). **D,** Violin plots showing the ICN1 ChIP-seq Log_2FC for all ICN1 peaks and ICN1 peaks that overlap with dynamic ETS1 peaks. **E,** Violin plots showing the ZMIZ1 ChIP-seq Log_2FC of all ZMIZ1 peaks or ZMIZ1 peaks that overlap with dynamic ETS1 peaks. **F,** ETS1, RBPJ, and H3K27ac ChIP-seq tracks at the N-ME (also see purple box in Fig. 5J), Notch-*MYB* enhancer (also see thick green box in Fig. 5K), Notch-*HES1* promoter, Notch-*NOTCH3* enhancer, and the Notch-*DTX1* enhancer. RBPJ peaks within black and green boxes gave P < 0.05 for both shETS1 comparisons. "a" and "b" are biological replicates (****, P < 0.0001).

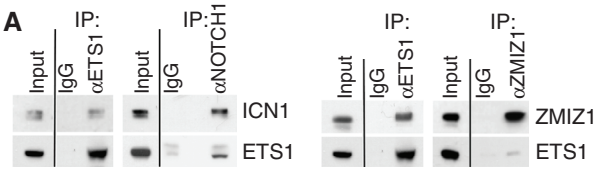

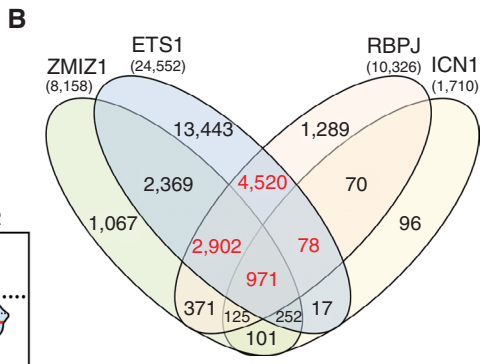

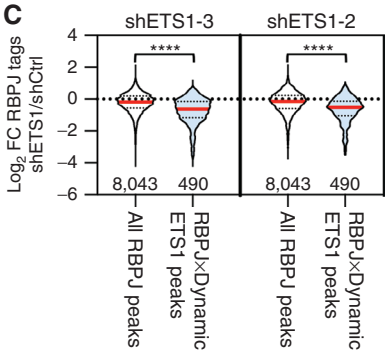

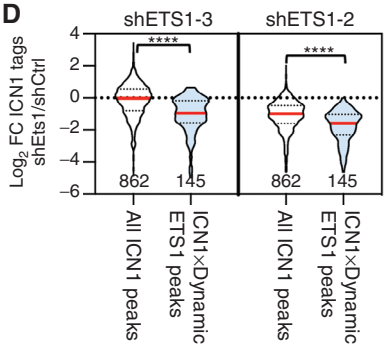

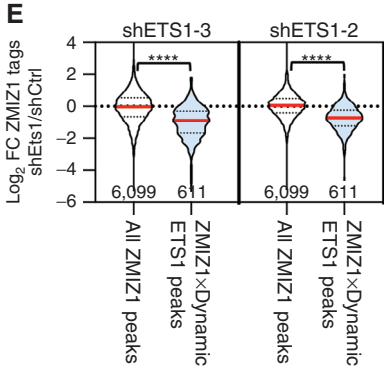

De novo motif analysis of 65 RBPJ peaks that cobind dynamic ETS1 peaks and change with FDR<0.1 for shCtrl vs. shETS1				Known motif analysis ($N = 65$) (FDR<0.1)		Known motif analysis ($N = 425$) (FDR>0.1)	
Rank	*De novo* motif	*P*-value	%sites	*P*-value	%sites	*P*-value	%sites
1	ETS	1E-31	40%	1E-21	40%	1E-48	20%
2	GATA	1E-22	52%	1E-17	43%	1E-25	17%
3	ETS-RUNX	1E-19	24%	1E-23	31%	1E-19	23%
4	bHLH	1E-11	38%	1E-05	35%	1E-05	17%
5	RBPJ	1E-10	54%	1E-02	29%	1E-02	20%

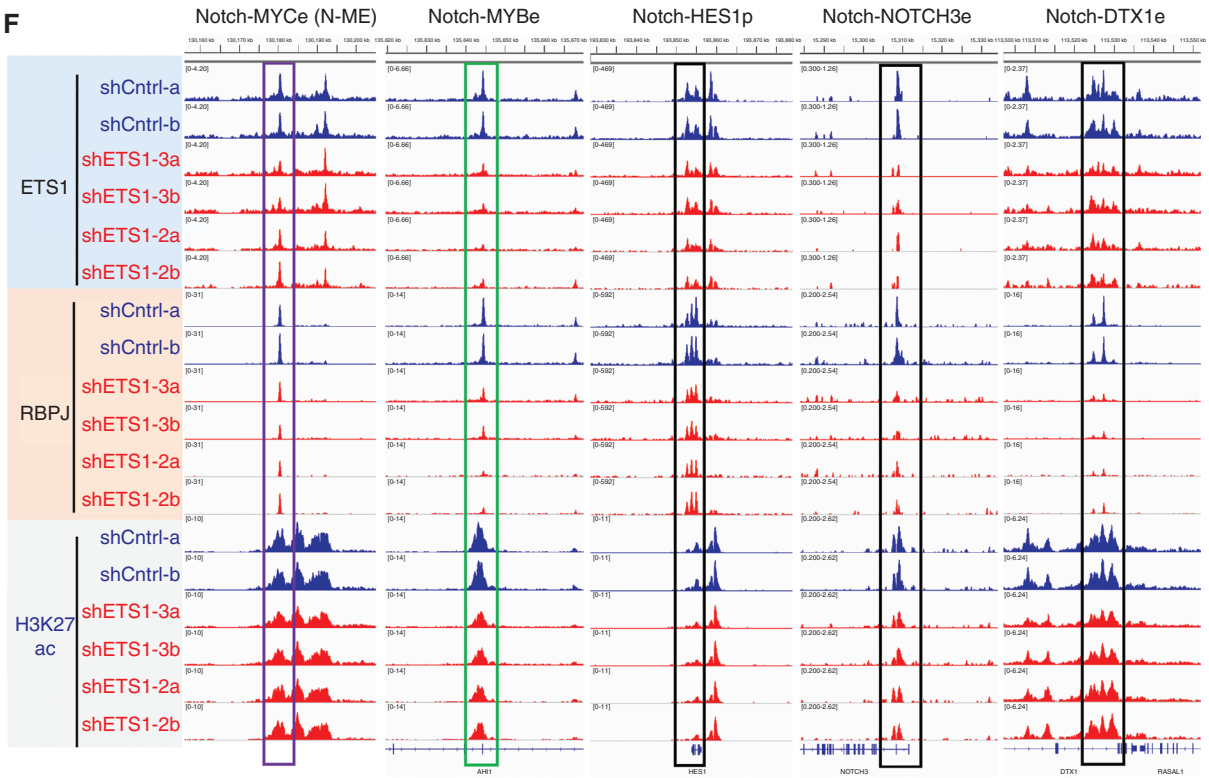

addition, we verified interactions between ETS1 and ZMIZ1, a context-dependent direct transcriptional cofactor of Notch1 (33, 46). Next, we performed ICN1, RBPJ, and ZMIZ1 ChIP-seq in control and shETS1-transduced THP-6 cells. These analyses identified 971 sites where ETS1, ZMIZ1, ICN1, and RBPJ peaks overlapped (Fig. 6B). Remarkably, 94% of overlapping ICN1 and RBPJ peaks contained an overlapping ZMIZ1 peak. Moreover, 35% and 28% of ETS1 peaks were cobound by RBPJ and ZMIZ1, respectively. In contrast, 77%, 73%, and 85% of ICN1 peaks were cobound by ETS1, RBPJ, and ZMIZ1, respectively. Furthermore, analysis of the 24,552 THP-6 ETS1 binding sites with ETS1, NOTCH1, RBPJ, and H3K27ac peaks in CUTLL1 and JURKAT cells revealed largely overlapping signals (Supplementary Fig. S6B and S6C). These results support that ETS1 binds NOTCH1 and cooccupies Notch complex binding sites.

ETS1 Facilitates Recruitment of Notch Complex Members and H3K27ac Deposition at Response Elements Enriched for GATA Factor Binding Motifs

Because ETS1 and NOTCH1 cobind chromatin and physically interact, we next asked, does ETS1 facilitate the recruitment of Notch complex members to chromatin? To answer this question, we investigated whether ETS1 deprivation could reduce RBPJ occupancy at sites where RBPJ peaks overlap with dynamic ETS1 peaks. Accordingly, ETS1 deprivation reduced read counts of RBPJ peaks that overlapped with dynamic ETS1 peaks compared with all RBPJ peaks (Fig. 6C, top). Mean RBPJ ChIP-seq Log_2FC differences were −0.517 and −0.436 by shETS1-3 and shETS1-2 compared with controls, respectively. Similarly, ETS1 deprivation reduced read counts of ICN1 and ZMIZ1 peaks that overlapped with dynamic ETS1 peaks compared with all ICN1 and ZMIZ1 peaks, with mean Log_2FC differences of −0.895 and −0.665 for ICN1 (Fig. 6D) and −0.921 and −0.780 for ZMIZ1 (Fig. 6E) by shETS1-3 and shETS1-2 compared with controls, respectively. Consistently, metagene plots showed that ETS1 deprivation reduced average read counts of RBPJ and ICN1 peaks that overlapped with dynamic ETS1 peaks (Supplementary Fig. S6E) compared with all RBPJ and ICN1 binding sites (Supplementary Fig. S6D). We conclude from these observations that ETS1 can facilitate the recruitment of Notch complex members to a subset of the regulatory sites controlling the transcription of Notch targets in T-ALL.

To better understand the mechanisms by which ETS1 facilitates recruitment of RBPJ to chromatin, we first defined "dynamic RBPJ peaks" as sites with differential RBPJ read counts following ETS1 knockdown (FDR < 0.1). Next, we performed motif analysis on dynamic ETS1 peaks that overlapped with dynamic RBPJ peaks. Similar to what we found for dynamic ETS1 peaks associated with differential H3K27ac signals (Supplementary Fig. S5L), a GATA family motif was the top-ranked non-ETS motif present in these locations. Interestingly, this GATA family motif was more closely associated with dynamic ETS1 peaks that overlapped with dynamic RBPJ peaks than dynamic ETS1 peaks that overlapped with nondynamic RBPJ peaks (43% vs. 17%; P = 1E-3; Fig. 6C, bottom). Similar associations with GATA3 were found for dynamic ICN1 peaks (P = 1E-2; Supplementary Fig. S6F) and dynamic ZMIZ1 peaks (P = 1E-10; Supplementary Fig. S6G). These data suggest that ETS1 cooperates with GATA3 to facilitate the recruitment of Notch factors to transcriptional control sites.

Because the Notch complex is known to facilitate H3K27ac deposition, we wondered whether ETS1 deprivation would weaken H3K27ac signals at dynamic ETS1 sites where RBPJ binding was reduced. In support of this hypothesis, ETS1 knockdown significantly reduced H3K27ac read counts at dynamic ETS1 peaks that overlap with dynamic RBPJ peaks compared with all dynamic ETS1 sites (Fig. 5I). H3K27ac ChIP-seq mean Log_2FC differences were −0.292 and −0.152 for shETS1-3 and shETS1-2 compared with controls, respectively. Similar results were found for dynamic ZMIZ1 peaks. We next considered the possibility that ETS1 recruits Notch to response elements that regulate shared NOTCH1/ETS1 target genes (Fig. 5D and F; Supplementary Fig. S5H). To test this possibility, we examined ETS1, RBPJ, and H3K27ac ChIP-seq tracks at Notch-bound response elements of *MYC* (N-ME), *MYB* (Notch-MYBe), *HES1* (Notch-HES1p), *NOTCH3* (Notch-NOTCH3e), and *DTX1* (Notch-DTX1e; Fig. 6F). ETS1 knockdown in THP-6 cells reduced RBPJ and H3K27ac read counts at the Notch-MYBe, Notch-HES1p, Notch-NOTCH3e, and Notch-DTX1e enhancers, but not N-ME. In contrast, ETS1 knockdown significantly reduced RBPJ signals at the N-ME in CEM cells (Supplementary Fig. S6H and S6I). These results further support that ETS1 might cooperate with GATA3 to facilitate recruitment of Notch to activate chromatin.

Ets1 Deprivation Sensitizes Leukemic Cells to Notch Inhibition

Several strategies have been proposed to maximize the therapeutic activity of anti-Notch therapies, including the combination of a GSI with agents targeting critical effectors downstream of Notch (43, 47, 48). Because our data show that ETS1 promotes MYC and mTOR (Supplementary Fig. S5A; Supplementary Table S1), two major oncogenic pathways downstream of NOTCH1 (48, 49), we wondered whether suppressing Ets1 signals might confer increased sensitivity to low doses of GSI. To test this possibility, we knocked down ETS1 in human T-ALL cell lines and treated them with a partially inhibitory dose of GSI (0.2 μmol/L; Supplementary Fig. S7A). As expected, partial Notch inhibition had only modest effects on the growth of GSI-sensitive cell lines (Supplementary Fig. S3H–S3J). ETS1 deprivation sensitized five of six cell lines to partial Notch inhibition, including all three GSI-resistant lines (CEM, THP-6, and JURKAT; Fig. 3C and D; Supplementary Fig. S3H, S3J, and S3L). Consistently, ETS1 knockdown and NOTCH1 deprivation cooperatively reduced *MYC* expression in THP-6 cells (Fig. 7A). Moreover, *Ets1* deletion and Notch inhibition with a GSI in Notch-induced *Rosa26CreER*^{T2} *Ets1*$^{f/f}$ murine T-ALL cells cooperatively downregulated *Myb* and *Dtx1* expression (Fig. 7B–D). In addition, and of therapeutic relevance, *in vivo* deletion of *Ets1* by tamoxifen treatment in this model enhanced the antileukemic effects of intermittent GSI dosing, resulting in reduced peripheral blood T-ALL blasts and increased survival compared with controls (Fig. 7E–H; Supplementary Fig. S7B). In all, these results support a therapeutic role for Ets1 inhibition in combination with anti-Notch1 therapies for the treatment of T-ALL.

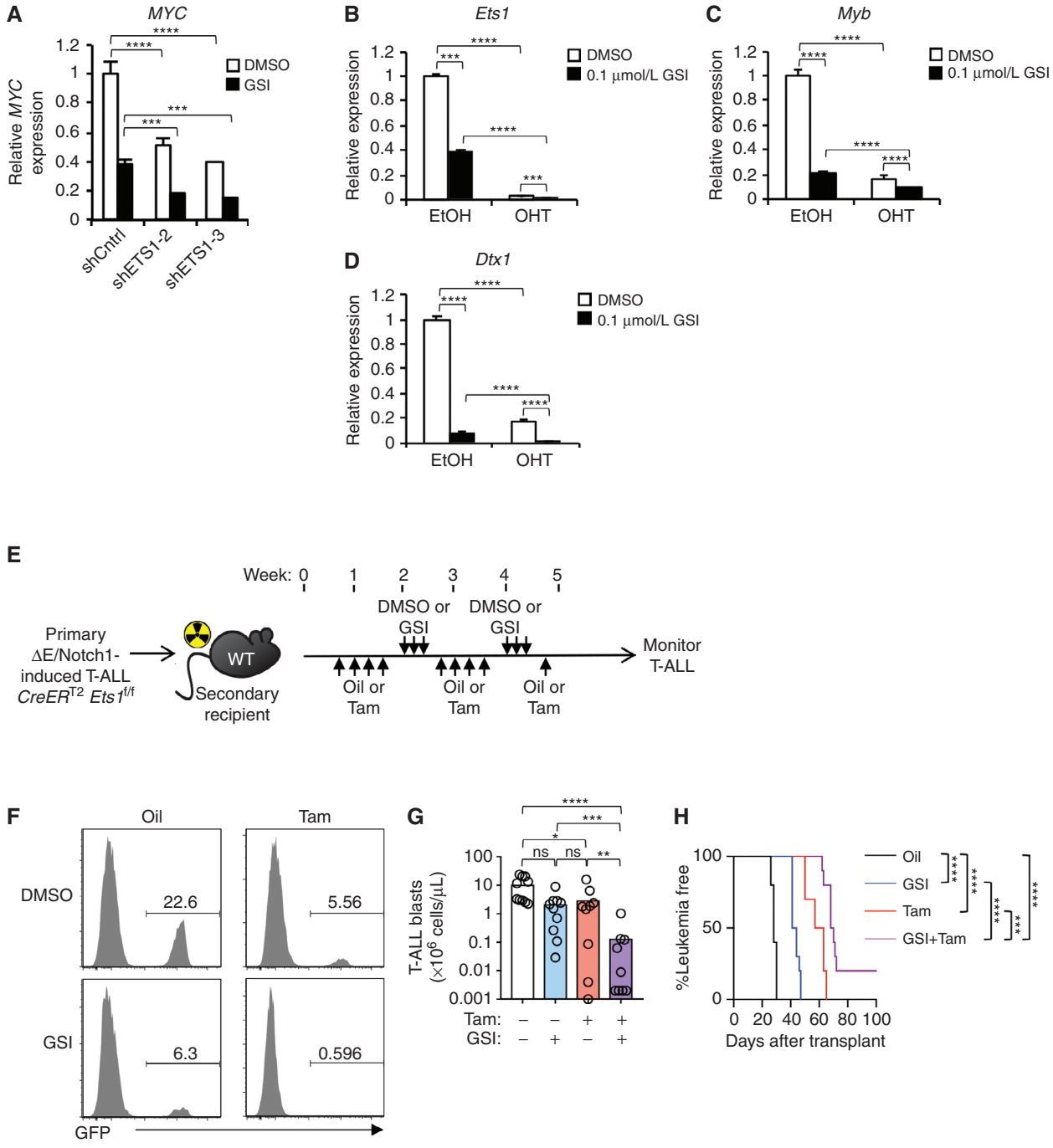

Figure 7. Ets1 deprivation sensitizes Notch-activated T-ALLs to the pan-Notch inhibitor GSI. **A,** Relative *MYC* expression in THP-6 cells transduced with shETS1 for 4 days and treated with GSI (DBZ, 1 μmol/L) 1 day prior to harvest. Expression of *Ets1* (**B**), *Myb* (**C**), and *Dtx1* (**D**) in murine *Rosa26CreER*^{T2} *Ets1*$^{f/f}$ cells (#643; GFP-positive T-ALL cell content 99.5%) treated with 12 nmol/L OHT to induce *Ets1* deletion for 42 hours ± low-dose GSI for 18 hours (DBZ, 0.1 μmol/L). **E–H,** Experimental strategy to study effects of combinatorial effects of Ets1/Notch deprivation on *in vivo* maintenance of murine ΔE/Notch1-induced T-ALL (#182; **E**). GSI, 10 μmol/kg DBZ; Tam, 25 mg/kg tamoxifen. Representative flow cytometric plots (**F**) and peripheral blood GFP$^+$ T-ALL cell counts (**G**) at 26 days posttransplant, and survival curves (**H**) (ns, not significant; *, $P < 0.05$; **, $P < 0.01$; ***, $P < 0.001$; ****, $P < 0.0001$).

DISCUSSION

During T-ALL transformation, Notch1 can become supraphysiologically activated or "hijacked," leading to widespread, intense expression of cleaved intracellular Notch1 (50). Current models support that Notch in turn hijacks its normal cellular partners including the cobinding transcription factors that it normally relies upon to promote T-cell development. In this context, such "Notch-collaborating" transcription factors might comprise new vulnerabilities in Notch-dependent cancers like T-ALL. These concepts are clinically relevant as continuous pan-Notch inhibition with GSI is poorly tolerated (43).

Here, we present evidence that Ets1 is a Notch-collaborating transcription factor and a potential therapeutic target in T-ALL. Using mouse models, we show that *Ets1* inactivation resembled the Notch1 inhibition phenotype by impairing ETP specification and the DN-to-DP transition, which are the two major Notch-dependent steps during early T-cell development. *Ets1* inactivation also impaired leukemic proliferation and Notch-induced gene expression in complementary mouse and human models of Notch-activated T-ALL. Accordingly, ChIP-seq analyses of T-ALL cells showed that approximately 80% of ICN1/RBPJ sites were cooccupied by ETS1. Compared with Notch inhibition, the effects of *Ets1* inactivation were strong in T-cell precursors or T-ALL cells but relatively weak in the intestine. Thus, Ets1 might have more substantial Notch-collaborating functions in the context of T-cell development and leukemogenesis than in the context of intestine stem cell differentiation.

It is worth noting that outside the T-cell compartment Ets1 plays a role in the maturation of other hematopoietic cells, such as B cells (31, 39, 42, 51–59). Thus, even though the effects of Ets1 on thymopoiesis are cell autonomous (17, 18) and B cells are dispensable for early T-cell development, it cannot be ruled out that some effect of *Ets1* inactivation in non–T-cell hematopoietic populations could influence the thymic phenotypes described here.

Functional analysis of ETS1 binding to chromatin sites in T-ALL revealed that only a minority of ETS1 peaks were suppressed upon ETS1 knockdown (dynamic ETS1 peaks). This finding is reminiscent of an earlier study showing that fewer than 10% of NOTCH1 peaks in CUTLL1 cells were dynamic when switching between Notch-on and Notch-off states (15). Like dynamic ETS1 peaks, dynamic NOTCH1 peaks were associated with differential H3K27ac read counts (15). For ETS1, our motif analyses suggest that dynamic peaks might signify a class of high-confidence binding sites that are highly sensitive to ETS1 dose reduction. In contrast to the high percentage of ICN1/RBPJ peaks that are cooccupied by ETS1, a much smaller percentage of ETS1 peaks were cooccupied by ICN1/RBPJ. Consistently, we identified several ETS1 target genes that, to our knowledge, have not been linked to dynamic NOTCH1 peaks or implicated as direct NOTCH1 target genes in publicly available T-ALL gene expression screens. Many of these genes, such as *GATA3, LYL1, PTPN11, LMO2, LCK*, and *HHEX*, have prominent roles in early T-cell development and leukemia transformation.

ETS1 loss often reduced H3K27ac read counts without affecting ICN1/RBPJ binding. However, we observed a small subgroup of ETS1 sites containing GATA motifs where ETS1 knockdown reduced ICN1/RBPJ binding and strongly reduced H3K27ac tags. Of note, this is a discrete feature suggestive of a strong functional interaction, as GATA motifs were uncommonly associated with ETS1 peaks (~15% of total). Combined with our observations of protein–protein interactions between ETS1 and NOTCH1 in two T-ALL cell lines, these data suggest the possibility of context-dependent transcriptional complexes that stabilize NOTCH1 complex interactions with chromatin (Supplementary Fig. S8). GATA3 is the predominant GATA family member expressed in T-ALL cells and is the only GATA family member expressed in the cell line we analyzed by ChIP-seq. It is possible that GATA3 might act as a scaffold linking ETS1 to the NOTCH1 complex. GATA3 pioneering factor activity can facilitate nucleosome eviction at the N-ME to promote transcription factor binding (12). Thus, GATA3-driven chromatin remodeling might help other proteins "connect" ETS1 to the Notch complex. Accordingly, our motif analysis suggests that transcription factors other than GATA3 are associated with dynamic changes of Notch factors and H3K27ac upon ETS1 knockdown. Moreover, because *GATA3* is an ETS1-induced gene, ETS1 might indirectly promote Notch complex recruitment and H3K27ac deposition through *GATA3* induction.

Therapeutically, our study demonstrates for the first time that it is possible to disengage activated Notch from its chromatin and gene expression functions in cancer cells without directly targeting the formation of the NOTCH1–RBPJ–MAML1 ternary complex. A corollary of these results is that combination strategies with anti-ETS1 and anti-Notch agents could synergize to enhance the antileukemic effects of Notch suppression. Finally, our study supports a model in which Notch-collaborating partner transcription factors like Ets1 create a favorable chromatin context for Notch1 to activate a subset of response elements. This evolutionary conserved principle already present in *Drosophila* (9) can be relevant to human disease as we show that context dependence through Ets1 could be exploited to oppose parts of the Notch downstream pathway in cancer with less toxicity than pan-Notch inhibitors. Moreover, given emerging data supporting a role for ETS1 in tumors such as breast, ovarian, and colon cancer (60) that are Notch dependent (1), our findings raise the possibility that ETS1 could cooperate with Notch to drive transformation in a diverse number of human cancers.

METHODS

Mice

C57BL/6 mice ranging from 4 weeks to 8 weeks of age were obtained from Taconic for bone marrow transplantation experiments. *Rosa26CreER*^{T2} *Ets1*$^{f/f}$ mice were generated by crossing *Ets1*$^{f/f}$ mice (M.C. Ostrowski; submitted for publication) with *Rosa26CreER*^{T2} mice (Jackson). *Rosa26CreER*$^{T2\text{-alt}}$ *Ets1*$^{f/f\text{-alt}}$ mice were generated by crossing *Ets1*$^{f/f\text{-alt}}$ mice (39) with *Rosa26CreER*$^{T2\text{-alt}}$ mice (40). The "alt" term was used to avoid confusion with the Jackson/Ostrowski *Rosa26CreER*^{T2} *Ets1*$^{f/f}$ mouse model described above. In *Ets1*$^{f/f}$ and *Ets1*$^{f/f\text{-alt}}$ mice, the *Ets1* conditional allele was constructed by flanking exons 7 and 8 with loxP sites. *Ets1*$^{p/p}$ mice, a gift from Dr. Garrett-Sinha (University at Buffalo, Buffalo, NY), were described previously (42).

In these mice, the exons 3 and 4 of *Ets1* (containing the PNT domain) were deleted, thus creating a hypomorphic "p" allele (31). *Notch1*$^{f/f}$ and *VavCre* (also known as "*Vav1-iCre*") mice were obtained from The Jackson Laboratory. *VillinCreER*^{T2} mice were obtained from S. Robine, Institut Curie, Paris, France (61). Mice used for T-cell developmental studies were 5 to 8 weeks of age. Mice used for *Rosa26-CreER*^{T2} and *VillinCreER*^{T2} experiments were 8 to 12 weeks old. Per animal protocol, mice were sacrificed when weight dropped to 80% or less of starting weight. All mouse experiments were performed according to NIH guidelines with approved protocols from the Institutional Animal Care and Use Committees at the University of Michigan (Ann Arbor, MI) and Columbia University Medical Center (New York, NY). A summary of the mice used is provided in Supplementary Table S5.

Histologic Analysis

Paraffin sections (5 μm) were stained with periodic acid-Schiff (PAS)/Alcian Blue (AB; Newcomer Supply) to assess mucin-containing goblet cells. PAS/AB-stained images from mouse intestines were quantified for proportion of blue staining (blue stained region in μm/total villus region in μm) using ImageJ software (NIH, Bethesda, MD). Villi length and crypt depth were traced and analyzed using the Measure tool. All quantitative analyses of the intestinal histology were performed by an observer who was blinded to the genotypes and treatment of the mice.

Cell Lines

Jurkat cells were provided by Jon Aster (Harvard University, Boston, MA). CEM cells were CEM/SS (a subclone of CCRF-CEM), which were provided by Katherine Collins (University of Michigan, Ann Arbor, MI). THP-6, DU.528, MOLT4, DND-41, and SUP-T1 cells were provided by Andrew Weng (Terry Fox Laboratory, Vancouver, BC, Canada). THP-6 is a GSI-resistant LYL1/LMO2-type T-ALL that expresses ICN1 (33, 46). HPB-ALL cells were obtained from DSMZ. LOUCY cells were obtained from ATCC. OP9-DL4 cells were provided by J.C. Zuniga-Pflucker (University of Toronto, Toronto, Ontario, Canada). Six hundred forty-three cells were established from a primary *Rosa26-CreER*^{T2} *Ets1*$^{f/f}$ splenic tumor. In these cells, *Ets1* can be deleted *in vitro* via the administration of 4-hydroxytamoxifen. All human cell lines were authenticated using STR analysis prior to use (Genetica Corporation). All cell lines were cultured less than 3 months after resuscitation and tested for contaminants using MycoAlert (Lonza) every 1 to 3 months to ensure they were free of *Mycoplasma* contamination.

Cell Culture Conditions

T-ALL cell lines were grown in RPMI1640 (Invitrogen) supplemented with 10% FBS (Hyclone or Gibco), 2 mmol/L L-glutamine, 2-mercaptoethanol [0.0005% (v/v), Sigma], penicillin, and streptomycin. Two hundred ninety-three T cells were maintained in DMEM (Invitrogen) with the same supplements except 2-mercaptoethanol. Cells were grown at 37°C under 5% CO_2. Retroviral and lentiviral transduction of T-ALL cells and sorting or selection were performed as described previously (62, 63). DBZ (GSI) was obtained from EMD chemicals (for *in vitro* studies) or Syncom (for *in vivo* studies). 4-hydroxytamoxifen was obtained from Sigma. For knockdown experiments, puromycin (Sigma) was added to transduced cell cultures 48 hours after transduction.

Flow Cytometry

Cells were stained on ice in PBS containing 2% FBS, 10 mmol/L HEPES, and 0.02% NaN_3 after blocking with rat and mouse IgG (Sigma). Flow cytometry antibodies were obtained from BioLegend or eBioscience (Supplementary Table S6). Samples were analyzed on an LSR Fortessa flow cytometer or sorted using a FACSAria II (BD Biosciences). Dead cells were excluded using 7-aminoactinomycin D (7-AAD) or 4′,6-diamidino-2-phenylindole (DAPI). Intracellular staining was performed using the BD Cell Fixation/Permeablization Kit (BD Biosciences, catalog no. 554714). Data were analyzed using FlowJo (Tree Star). Cell-cycle analysis was performed by administering 1 mL of propidium iodide stain solution (PI, 20 μg/mL and DNase free RNase A, 100 μg/mL) to the freshly collected cells from primary tissues and analyzed by FACS within 30 minutes. Annexin V/7-AAD staining was performed on fresh cells according to manufacturer's specifications (BD Biosciences) for apoptosis and cell death analysis. Each experimental condition was run in triplicate. The values displayed are representative of three biological replicates. All data acquisition was performed on BD-FACS Canto and analyzed using FlowJo analysis software (Tree Star).

Human Patient/PDX Expression Data

The human patient data in Supplementary Fig. S4B and S4C were based upon data generated by the Therapeutically Applicable Research to Generate Effective Treatments (TARGET; https://ocg.cancer.gov/programs/target) initiative, phs000218. The ALL project team was headed by Stephen P. Hunger, MD, at the University of Colorado Cancer Center (Denver, CO). The database of Genotypes and Phenotypes (dbGaP) substudy ID is phs000463/phs000464. The data used for this analysis are available at https://portal.gdc.cancer.gov/projects. Heatmap of Ets family member expression was generated in the ProXe database app (https://proxe.shinyapps.io/PRoXe/) using only the T-ALL PDXs available in the database.

PDX Experiments

PDXs (IDs: M71, BCAT17802-V2, and BCAT82114-V1) were obtained from Andrew Weng (Terry Fox Laboratory, Vancouver, BC, Canada). Deidentified human samples were obtained and used with appropriate institutional approval (University of Michigan Institutional Review Board, UBC/BCCA Research Ethics Board, Institutional Review Board of the Institut Universitaire d'Hématologie/Université Paris Diderot) and written informed consent under guidelines established by the Declaration of Helsinki. PDXs were expanded by injecting them into nonirradiated NOD-*scid*-IL2Rgamma^{null} (NSG) mice and then harvesting spleens at time of morbidity. Human-specific antibodies against CD45 and CD7 were used to discern human T-ALL lymphoblasts and differentiated from mouse cells with antibodies against murine CD45. Live-frozen PDX aliquots were thawed and cocultured on irradiated OP9-DL4 stromal cells in Iscove modified Dulbecco's media (Invitrogen) supplemented with human stem cell factor (hSCF, PeproTech, #300-07, 50 ng/mL), human insulin-like growth factor (hIGF, PeproTech, #100-11, 10 ng/mL), human IL2 (hIL2, PeproTech, #200-02, 10 ng/mL), murine IL7 (mIL7, PeproTech, #217-17, 10 ng/mL), and SR-1 (Cayman, 0.57 μmol/L). PDXs were transduced with concentrated lentivirus and plated on irradiated OP9-DL4 cells for *in vitro* growth assay. Cells were analyzed via FACS for YFP and replated on freshly irradiated OP9-DL4 cells every 3 days; "YFP^{hi}" cells were defined as DAPI$^-$, hCD45$^+$, and top 25% of YFP expression. Transduced YFP^{hi} PDX cells were sorted and injected (20K cells/mouse) into NSG mice for leukemia initiation studies. The development of leukemia was monitored by flow cytometry (hCD45, YFP). Once the mice were moribund, spleen cells were harvested and analyzed by flow cytometry and qRT-PCR.

Quantitative PCR

The DNA-based qPCR assay to assess *Ets1* deletion efficiency used deletion primers that bind Intron 5 between the loxP sequences and control primers that bind Intron 3 outside the loxP sequences. qPCR was quantified using standard curve constructed from serial dilutions of spleen DNA of an Ets1$^{f/f}$ mouse, thus containing decreasing amounts of *Ets1* floxed DNA. For qRT-PCR, total RNA was prepared using the RNeasy Plus Mini kit (Qiagen) according to the manufacturer's protocol. Random-primed total RNAs (0.5 μg) were reverse transcribed

with SuperScript II (Invitrogen). Transcripts were amplified with either TaqMan Universal PCR Master Mix or Power Sybr Green PCR Master Mix (Applied Biosystems) on the Applied Biosystems StepOnePlus (Applied Biosystems). Relative expression of target genes compared with the control was calculated using the delta-delta cycle threshold method with the expression of EF1A or 18S as an internal reference. See Supplementary Table S6 for information on the primers that were used.

ChIP-seq Library Preparation and Sequencing

ChIP chromatin was prepared as described above from THP-6 cells in biological duplicates with shControl (SHC002, Sigma), shETS1-3 (TRCN00005591, Sigma), or shETS1-2 (TRCN00001916, Sigma), treated at 48 hours with puromycin, and harvested after an additional 48 hours. ChIP-seq libraries were prepared as described previously (64). Briefly, ChIP DNA was end-repaired (End-It, Epicentre), A-tailed (Klenow fragment 3′→5′ exo-, New England Biolabs), and ligated to barcoded Illumina adaptors (Quick T4 DNA ligase, NEB; adaptors produced by KAPA). Each reaction was followed by clean-up with SPRI beads (AmpureXP, Beckman Coulter). Ligation products were amplified by 14 cycles of PCR with Illumina indexing primers and PFU Ultra II HS PCR mix (Agilent). Library size selection for 300 to 600 bp chromatin was performed using two-step SPRI bead selection (AmpureXP, Beckman Coulter). Library size was confirmed via Tapestation D1000 (Agilent). Final libraries were sequenced with 75-cycle paired end (38 bp × 2) on a Nextseq (Illumina) according to manufacturer's protocols.

ChIP-seq Alignment, Filtering, Track Generation, Peak Calling, and Overlaps

Reads were aligned to the hg19 genome assembly using bwa-aln (bwa version 0.7.12). Data were filtered to remove PCR duplicates and reads mapping to >2 genomic sites. All peak sets were also post-filtered for known ENCODE blacklist regions (available at http://hgdownload.cse.ucsc.edu/goldenpath/hg19/encodeDCC/wgEncodeMapability/wgEncodeDacMapabilityConsensusExcludable.bed.gz). Filtered bam files were marked as "pruned bam files." Next, bigwig display files were generated with igvtools count and deepTools bamCoverage. Bed peak files were generated with HOMER findPeaks ("style-factor" for transcription factors). Scaling for all ChIP-seq tracks in the figures is equal to local paired-end fragment coverage × (1,000,000/totalCount). To determine overlaps between ETS1, NOTCH1, ZMIZ1, and RBPJ peaks, we first concatenated the two shControl bioreplicates for each transcription factor, using mergeBed in BEDTools. We then identified the total number of peaks for each transcription factor as well as the overlaps between the transcription factors using intersectBed in BEDTools. These data were then plotted in a Venn diagram using Microsoft Excel.

Identification of High-Confidence ETS1 Direct Target Genes

To identify high-confidence ETS1 direct target genes, we concatenated peaks from the two shControl ETS1 ChIP-seq biological replicates and merged overlapping ones using mergeBed in BEDTools. We performed differential binding analysis comparing shETS1-3 or shETS1-2 versus shControl using DiffBind (2.14.0; http://bioconductor.org/packages/release/bioc/vignettes/DiffBind/inst/doc/DiffBind.pdf). Because DiffBind can use either DESeq2 or edgeR to do normalization and differential tests, it was run twice to generate results from both methods. The DESeq2 method was used, as it identified more differentially regulated peaks than edgeR. We defined "dynamic ETS1 peaks" as ETS1 peaks that gave FDR < 0.1 for the shControl versus shETS1-3 comparison and the shControl versus shETS1-2 comparison. Next, we extracted from the RNA-seq data in THP-6 cells (above) the DEGs that were shared between the shControl versus shETS1-3 and shControl versus shETS1-2 comparisons requiring Q < 0.05 in both and the changing direction to be the same. We extracted TADs based on Hi-C data in CUTLL1 cells (GSE134761; ref. 65). For each dynamic ETS1 peak, we found the TAD(s) it intersected with and the DEGs that intersected with the same TAD(s) using intersectBed in BEDTools. TAD boundaries were first extended to cover the flanking gaps. These DEGs were designated as high-confidence direct NOTCH1 target genes as they were linked to at least one ETS1 dynamic peak within the same TAD as the DEG. Dynamic ETS1 peaks that overlapped with two adjacent TADs were assigned to both TADs. DEGs that overlapped with two adjacent TADs were assigned to both TADs. We also extracted H3K27ac Hi-ChIP intervals in CUTLL1 cells (GSE134761; ref. 65). We filtered the DEGs to include only those DEGs with TSS within Hi-ChIP intervals that were linked to another Hi-ChIP interval that contained at least one dynamic ETS1 peaks using R version 3.6.1 with tidyverse (1.3.0). The DEGs linked to dynamic ETS1 peaks within the same TAD and the filtered DEGs that were additionally linked to dynamic ETS1 peaks through H3K27ac Hi-ChIP are listed in separate tabs in Supplementary Table S4.

Comparative ChIP-seq Analysis

To determine differential binding of Notch complex members and differential H3K27ac signals, we created a set of union intervals by merging the bed files for the ETS1, NOTCH1, RBPJ, and ZMIZ1 peaks. Narrow windows for transcription factors were 200 bp, centered on the union interval peak. Broad windows for H3K27Ac were 2,000 bp, centered on the union interval peak. For each of the union intervals, we found the intersection counts and overlap fraction from each factor's peak sets, using annotateBed in BEDTools. We used annotatedPeaks.pl in HOMER to calculate normalized tag count distribution surrounding the interval centers. DiffBind (2.14.0) was run twice to generate results using both DESeq2 and edgeR methods. DESeq2 was used for ETS1 and H3K27Ac ChIP-seq data. edgeR was used for ICN1, RBPJ, and ZMIZ1 ChIP-seq data. Binding/H3K27ac quantitation and differential binding/H3K27ac analysis were then obtained. For violin plot analyses, we defined transcription factor peaks as union intervals that intersected with at least one peak of that transcription factor in at least one control bioreplicate. Unless otherwise indicated, we defined "dynamic ETS1 peaks" as union intervals that intersected with at least one ETS1 peak in at least one control bioreplicate and that gave FDR < 0.1 for the shControl versus shETS1-3 comparison and the shControl versus shETS1-2 comparison. Likewise, we defined dynamic ICN1, RBPJ, and ZMIZ1 peaks as union intervals that intersected at least one peak of that factor in at least one control bioreplicate and gave FDR < 0.1 for the shControl versus shETS1-3 comparison and the shControl versus shETS1-2 comparison. To generate metagene plots, two interval sets were selected: (i) "All Peaks" = intervals that intersect with at least one peak of that factor in all of the shETS1 bioreplicates (shETS1-3 and shETS1-2) or intersect with at least one peak of that factor in both shControl replicates and (ii) intervals from (i) that intersect with at least one dynamic ETS1 peak. To generate metagene plots in Supplementary Fig. S6D and S6E, we used annotatedPeaks.pl in HOMER to calculate normalized tag count distribution surrounding the interval centers for each of the two groups (i and ii) above and plotted them using R. We also calculated the normalized tag count distribution for (iii) the broader H3K27ac intervals that intersected with at least one ETS1 peak in all of the shETS1 bioreplicates (shETS1-3 and shETS1-2) or intersected at least one ETS1 peak in both shControl replicates and (iv) broad intervals from (iii) that intersected with at least one dynamic ETS1 peak. Volcano plots for ETS1 ChIP-seq differential binding were generated using R Version 3.6.1, with the following packages: tidyverse (1.3.0), ggrepel (0.8.1), extrafont (0.17), and stringr (1.4.0). *De novo* DNA motif enrichment analysis was performed with HOMER findMotifs, using findMotifsGenome.pl with a setting of -size 200.

The background peakset was HOMER generated and GC content normalized. Known motif analysis was performed with the HOMER motif library version 4.10.4, using two sets of peaks: (i) peaks identified as differentially bound by the given transcription factor in both the shETS1-3– and shETS1-2–treated cells (vs. shControl, FDR < 0.1) and (ii) peaks that were NOT identified as differentially bound by the given transcription factor in either the shETS1-3 or shETS1-2 comparison (vs. shControl, FDR > 0.1). To obtain *P* values for the enrichment of the GATA family motif in the first peakset versus the second peakset, we inputted the first peakset as the "target" peaks and the second peakset as the "background" peaks and the known motif Gata4(Zf)/Heart_Gata4_ChIP-seq (GSE35151) into the HOMER findMotifsGenome.pl command. *De novo* DNA motif analyses were also performed for all ETS1, ICN1, and RBPJ peaks (Supplementary Fig. S9).

Deposition of Sequences

The high-throughput sequencing and microarray data were deposited in the Gene Expression Omnibus database with accession GSE138660 for the superseries. Subseries include GSE138516 (ChIP-seq), GSE138659 (RNA-seq), and GSE138803 (microarray).

Disclosure of Potential Conflicts of Interest

A.C. McCarter reports grants from NIH (T32-GM007315, T32-GM007863, and F30-CA228228) during the conduct of the study. G. Della Gatta reports other from Regeneron Pharmaceuticals (currently an employee of Regeneron Pharmaceuticals studying the molecular basis of obesity and other metabolic syndromes) outside the submitted work. A. Melnick reports grants from NIH during the conduct of the study. J.K. Nalamolu reports grants from NIH during the conduct of the study. N. Kunnath reports grants from NIH (to institution, the University of Michigan) outside the submitted work. A. Rao reports other from Voxel Analytics, LLC (consulting) and grants from NIH, American Cancer Society (ACS), and Agilent Technologies outside the submitted work. L.C. Samuelson reports grants from NIH during the conduct of the study. M.C. Ostrowski reports grants from Medical University of South Carolina during the conduct of the study. A.A. Ferrando reports grants from NCI, NIH and Leukemia & Lymphoma Society during the conduct of the study and personal fees from Ayala Pharmaceuticals, SpringWorks Therapeutics, and Pfizer outside the submitted work. In addition, A.A. Ferrando has a patent for 20070077245 issued and with royalties paid from Pfizer, Merck; a patent for 20100087358 issued and with royalties paid from Pfizer, Merck; a patent for 20100093684 issued and with royalties paid from Pfizer; has patents for 20110118192, 8633179, and 8716233 issued; and his lab generated the CUTLL1 cell line, which is licensed to Novartis, EMD Millipore, and Applied Biological Materials. M.Y. Chiang reports grants from NIH, Rally Foundation for Childhood Cancer, Bear Necessities Pediatric Cancer Foundation Research (outside the submitted work), and Alex's Lemonade Stand Foundation (during the conduct of the study), and Rally Young Professionals; and grants, personal fees, and nonfinancial support from the University of Michigan. No potential conflicts of interest were disclosed by the other authors.

Authors' Contributions

A.C. McCarter: Formal analysis, funding acquisition, investigation, visualization, writing–original draft, writing–review and editing. **G. Della Gatta:** Formal analysis, investigation, visualization, writing–original draft, writing–review and editing. **A. Melnick:** Formal analysis, validation, investigation, writing–review and editing. **E. Kim:** Validation, visualization. **C. Sha:** Investigation, visualization. **Q. Wang:** Investigation, visualization. **J.K. Nalamolu:** Investigation, visualization. **Y. Liu:** Investigation, visualization. **T.M. Keeley:** Formal analysis, investigation, visualization, writing–review and editing. **R. Yan:** Investigation, visualization. **M. Sun:** Investigation. **R. Kodgule:** Investigation. **N. Kunnath:** Software, formal analysis. **A. Ambesi-Impiombato:** Software, formal analysis. **R. Kuick:** Data curation, software, formal analysis, writing–original draft, writing–review and editing. **A. Rao:** Supervision. **R.J.H. Ryan:** Conceptualization, resources, data curation, software, formal analysis, supervision, visualization, methodology, writing–original draft, writing–review and editing. **B.L. Kee:** Conceptualization, resources, supervision, funding acquisition, methodology, writing–original draft, writing–review and editing. **L.C. Samuelson:** Conceptualization, resources, supervision, funding acquisition, visualization, writing–original draft, writing–review and editing. **M.C. Ostrowski:** Conceptualization, resources, funding acquisition, methodology, writing–original draft, writing–review and editing. **A.A. Ferrando:** Conceptualization, formal analysis, supervision, funding acquisition, visualization, methodology, writing–original draft, writing–review and editing. **M.Y. Chiang:** Conceptualization, formal analysis, supervision, funding acquisition, visualization, methodology, writing–original draft, writing–review and editing.

Acknowledgments

The authors thank Weisheng Wu, Rebecca Tagett, Judy Opp, Melissa Coon, Yeonjoo Oh, and Amparo Serna Alarcon for invaluable assistance. M.Y. Chiang was supported by the NIH (R01CA196604 and R01AI136941-01), the Alex's Lemonade Stand Foundation, the Rally Young Professionals and the Rally Foundation for Childhood Cancer Research, and the Bear Necessities Pediatric Cancer Foundation. A.C. McCarter and A. Melnick were supported by NIH training grant T32-GM007315. A.C. McCarter was supported by 1F30CA228228-01. A.A. Ferrando was supported by NIH grants R35 CA210065, and P30 CA013696 (Transgenic Animal Shared Resource, Molecular Pathology Shared Resource, Genomics Shared Resource, Herbert Irving Comprehensive Cancer Center). Other support was provided to R. Kodgule (P30-CA46592), B.L. Kee (R01 AI106352), and L.C. Samuelson (R01-DK118023). The authors are grateful to T. Ludwig (The Ohio State University Comprehensive Cancer Center) for the Rosa26CreER$^{T2\text{-}alt}$ mouse.

The costs of publication of this article were defrayed in part by the payment of page charges. This article must therefore be hereby marked *advertisement* in accordance with 18 U.S.C. Section 1734 solely to indicate this fact.

Received February 24, 2020; revised May 22, 2020; accepted June 11, 2020; published first July 14, 2020.

REFERENCES

1. Miele L, Artavanis-Tsakonas S, editors. Targeting notch in cancer: from the fruit fly to the clinic. New York, NY: Springer Nature; 2018.
2. McCarter AC, Wang Q, Chiang M. Notch in leukemia. Adv Exp Med Biol 2018;1066:355–94.
3. Deangelo DJ, Stone RM, Silverman LB, Stock W, Attar EC, Fearen I, et al. A phase I clinical trial of the notch inhibitor MK-0752 in patients with T-cell acute lymphoblastic leukemia/lymphoma (T-ALL) and other leukemias. J Clin Oncol 2006;24:6585.
4. Krop I, Demuth T, Guthrie T, Wen PY, Mason WP, Chinnaiyan P, et al. Phase I pharmacologic and pharmacodynamic study of the gamma secretase (Notch) inhibitor MK-0752 in adult patients with advanced solid tumors. J Clin Oncol 2012;30:2307–13.
5. Tolcher AW, Messersmith WA, Mikulski SM, Papadopoulos KP, Kwak EL, Gibbon DG, et al. Phase I study of RO4929097, a gamma secretase inhibitor of Notch signaling, in patients with refractory metastatic or locally advanced solid tumors. J Clin Oncol 2012;30:2348–53.
6. van Es JH, van Gijn ME, Riccio O, van den Born M, Vooijs M, Begthel H, et al. Notch/gamma-secretase inhibition turns proliferative

cells in intestinal crypts and adenomas into goblet cells. Nature 2005;435:959–63.
7. Carulli AJ, Keeley TM, Demitrack ES, Chung J, Maillard I, Samuelson LC. Notch receptor regulation of intestinal stem cell homeostasis and crypt regeneration. Dev Biol 2015;402:98–108.
8. VanDussen KL, Carulli AJ, Keeley TM, Patel SR, Puthoff BJ, Magness ST, et al. Notch signaling modulates proliferation and differentiation of intestinal crypt base columnar stem cells. Development 2012;139:488–97.
9. Falo-Sanjuan J, Bray SJ. Decoding the Notch signal. Dev Growth Differ 2020;62:4–14.
10. Herranz D, Ambesi-Impiombato A, Palomero T, Schnell SA, Belver L, Wendorff AA, et al. A NOTCH1-driven MYC enhancer promotes T cell development, transformation and acute lymphoblastic leukemia. Nat Med 2014;20:1130–7.
11. Yashiro-Ohtani Y, Wang H, Zang C, Arnett KL, Bailis W, Ho Y, et al. Long-range enhancer activity determines Myc sensitivity to Notch inhibitors in T cell leukemia. Proc Natl Acad Sci U S A 2014;111:E4946–53.
12. Belver L, Yang AY, Albero R, Herranz D, Brundu FG, Quinn SA, et al. Gata3-controlled nucleosome eviction drives Myc enhancer activity in T-cell development and leukemia. Cancer Discov 2019;9:1774–91.
13. Hollenhorst PC, McIntosh LP, Graves BJ. Genomic and biochemical insights into the specificity of ETS transcription factors. Annu Rev Biochem 2011;80:437–71.
14. Garrett-Sinha LA. Review of Ets1 structure, function, and roles in immunity. Cell Mol Life Sci 2013;70:3375–90.
15. Wang H, Zang C, Taing L, Arnett KL, Wong YJ, Pear WS, et al. NOTCH1-RBPJ complexes drive target gene expression through dynamic interactions with superenhancers. Proc Natl Acad Sci U S A 2014;111:705–10.
16. Choi A, Illendula A, Pulikkan JA, Roderick JE, Tesell J, Yu J, et al. RUNX1 is required for oncogenic Myb and Myc enhancer activity in T-cell acute lymphoblastic leukemia. Blood 2017;130:1722–33.
17. Bories JC, Willerford DM, Grevin D, Davidson L, Camus A, Martin P, et al. Increased T-cell apoptosis and terminal B-cell differentiation induced by inactivation of the Ets-1 proto-oncogene. Nature 1995;377:635–8.
18. Muthusamy N, Barton K, Leiden JM. Defective activation and survival of T cells lacking the Ets-1 transcription factor. Nature 1995;377:639–42.
19. Rahman S, Magnussen M, Leon TE, Farah N, Li Z, Abraham BJ, et al. Activation of the LMO2 oncogene through a somatically acquired neomorphic promoter in T-cell acute lymphoblastic leukemia. Blood 2017;129:3221–6.
20. Sanda T, Lawton LN, Barrasa MI, Fan ZP, Kohlhammer H, Gutierrez A, et al. Core transcriptional regulatory circuit controlled by the TAL1 complex in human T cell acute lymphoblastic leukemia. Cancer Cell 2012;22:209–21.
21. Palii CG, Perez-Iratxeta C, Yao Z, Cao Y, Dai F, Davison J, et al. Differential genomic targeting of the transcription factor TAL1 in alternate haematopoietic lineages. EMBO J 2011;30:494–509.
22. Vanden Bempt M, Demeyer S, Broux M, De Bie J, Bornschein S, Mentens N, et al. Cooperative enhancer activation by TLX1 and STAT5 drives development of NUP214-ABL1/TLX1-positive T cell acute lymphoblastic leukemia. Cancer Cell 2018;34:271–85.
23. Bain G, Engel I, Robanus Maandag EC, te Riele HP, Voland JR, Sharp LL, et al. E2A deficiency leads to abnormalities in alphabeta T-cell development and to rapid development of T-cell lymphomas. Mol Cell Biol 1997;17:4782–91.
24. Winandy S, Wu P, Georgopoulos K. A dominant mutation in the Ikaros gene leads to rapid development of leukemia and lymphoma. Cell 1995;83:289–99.
25. Zhang J, Ding L, Holmfeldt L, Wu G, Heatley SL, Payne-Turner D, et al. The genetic basis of early T-cell precursor acute lymphoblastic leukaemia. Nature 2012;481:157–63.
26. Mullighan CG, Goorha S, Radtke I, Miller CB, Coustan-Smith E, Dalton JD, et al. Genome-wide analysis of genetic alterations in acute lymphoblastic leukaemia. Nature 2007;446:758–64.
27. Gutierrez A, Sanda T, Ma W, Zhang J, Grebliunaite R, Dahlberg S, et al. Inactivation of LEF1 in T-cell acute lymphoblastic leukemia. Blood 2004;115:2845–51.
28. Oikawa T, Yamada T. Molecular biology of the Ets family of transcription factors. Gene 2003;303:11–34.
29. Rothenberg EV, Ungerback J, Champhekar A. Forging T-lymphocyte identity: intersecting networks of transcriptional control. Adv Immunol 2016;129:109–74.
30. Tatarek J, Cullion K, Ashworth T, Gerstein R, Aster JC, Kelliher MA. Notch1 inhibition targets the leukemia-initiating cells in a Tal1/Lmo2 mouse model of T-ALL. Blood 2011;118:1579–90.
31. Wang D, John SA, Clements JL, Percy DH, Barton KP, Garrett-Sinha LA. Ets-1 deficiency leads to altered B cell differentiation, hyperresponsiveness to TLR9 and autoimmune disease. Int Immunol 2005;17:1179–91.
32. Eyquem S, Chemin K, Fasseu M, Bories JC. The Ets-1 transcription factor is required for complete pre-T cell receptor function and allelic exclusion at the T cell receptor beta locus. Proc Natl Acad Sci U S A 2004;101:15712–7.
33. Wang Q, Yan R, Pinnell N, McCarter AC, Oh Y, Liu Y, et al. Stage-specific roles for Zmiz1 in Notch-dependent steps of early T-cell development. Blood 2018;132:1279–92.
34. Wolfer A, Wilson A, Nemir M, MacDonald HR, Radtke F. Inactivation of Notch1 impairs VDJbeta rearrangement and allows pre-TCR-independent survival of early alpha beta lineage thymocytes. Immunity 2002;16:869–79.
35. Aster JC, Xu L, Karnell FG, Patriub V, Pui JC, Pear WS. Essential roles for ankyrin repeat and transactivation domains in induction of T-cell leukemia by notch1. Mol Cell Biol 2000;20:7505–15.
36. Pear WS, Aster JC, Scott ML, Hasserjian RP, Soffer B, Sklar J, et al. Exclusive development of T cell neoplasms in mice transplanted with bone marrow expressing activated Notch alleles. J Exp Med 1996;183:2283–91.
37. Weng AP, Nam Y, Wolfe MS, Pear WS, Griffin JD, Blacklow SC, et al. Growth suppression of pre-T acute lymphoblastic leukemia cells by inhibition of notch signaling. Mol Cell Biol 2003;23:655–64.
38. Schroeter EH, Kisslinger JA, Kopan R. Notch-1 signalling requires ligand-induced proteolytic release of intracellular domain. Nature 1998;393:382–6.
39. Zook EC, Ramirez K, Guo X, van der Voort G, Sigvardsson M, Svensson EC, et al. The ETS1 transcription factor is required for the development and cytokine-induced expansion of ILC2. J Exp Med 2016;213:687–96.
40. Guo K, McMinn JE, Ludwig T, Yu YH, Yang G, Chen L, et al. Disruption of peripheral leptin signaling in mice results in hyperleptinemia without associated metabolic abnormalities. Endocrinology 2007;148:3987–97.
41. Schnell SA, Ambesi-Impiombato A, Sanchez-Martin M, Belver L, Xu L, Qin Y, et al. Therapeutic targeting of HES1 transcriptional programs in T-ALL. Blood 2015;125:2806–14.
42. Barton K, Muthusamy N, Fischer C, Ting CN, Walunas TL, Lanier LL, et al. The Ets-1 transcription factor is required for the development of natural killer cells in mice. Immunity 1998;9:555–63.
43. Real PJ, Tosello V, Palomero T, Castillo M, Hernando E, de Stanchina E, et al. Gamma-secretase inhibitors reverse glucocorticoid resistance in T cell acute lymphoblastic leukemia. Nat Med 2009;15:50–8.
44. Chiang MY, Wang Q, Gormley AC, Stein SJ, Xu L, Shestova O, et al. High selective pressure for Notch1 mutations that induce Myc in T-cell acute lymphoblastic leukemia. Blood 2016;128:2229–40.
45. Palomero T, Lim WK, Odom DT, Sulis ML, Real PJ, Margolin A, et al. NOTCH1 directly regulates c-MYC and activates a feed-forward-loop transcriptional network promoting leukemic cell growth. Proc Natl Acad Sci U S A 2006;103:18261–6.
46. Pinnell N, Yan R, Cho HJ, Keeley T, Murai MJ, Liu Y, et al. The PIAS-like coactivator Zmiz1 is a direct and selective cofactor of Notch1 in T cell development and leukemia. Immunity 2015;43:870–83.
47. Sanchez-Martin M, Ambesi-Impiombato A, Qin Y, Herranz D, Bansal M, Girardi T, et al. Synergistic antileukemic therapies in NOTCH1-induced T-ALL. Proc Natl Acad Sci U S A 2017;114:2006–11.

48. Herranz D, Ambesi-Impiombato A, Sudderth J, Sanchez-Martin M, Belver L, Tosello V, et al. Metabolic reprogramming induces resistance to anti-NOTCH1 therapies in T cell acute lymphoblastic leukemia. Nat Med 2015;21:1182–9.
49. Weng AP, Millholland JM, Yashiro-Ohtani Y, Arcangeli ML, Lau A, Wai C, et al. c-Myc is an important direct target of Notch1 in T-cell acute lymphoblastic leukemia/lymphoma. Genes Dev 2006;20:2096–109.
50. Kluk MJ, Ashworth T, Wang H, Knoechel B, Mason EF, Morgan EA, et al. Gauging NOTCH1 activation in cancer using immunohistochemistry. PLoS One 2013;8:e67306.
51. Sunshine A, Goich D, Stith A, Sortino K, Dalton J, Metcalfe S, et al. Ets1 controls the development of B cell autoimmune responses in a cell-intrinsic manner. Immunohorizons 2019;3:331–40.
52. John S, Russell L, Chin SS, Luo W, Oshima R, Garrett-Sinha LA. Transcription factor Ets1, but not the closely related factor Ets2, inhibits antibody-secreting cell differentiation. Mol Cell Biol 2014;34:522–32.
53. Luo W, Mayeux J, Gutierrez T, Russell L, Getahun A, Muller J, et al. A balance between B cell receptor and inhibitory receptor signaling controls plasma cell differentiation by maintaining optimal Ets1 levels. J Immunol 2014;193:909–20.
54. Mayeux J, Skaug B, Luo W, Russell LM, John S, Saelee P, et al. Genetic interaction between Lyn, Ets1, and Btk in the control of antibody levels. J Immunol 2015;195:1955–63.
55. Russell L, John S, Cullen J, Luo W, Shlomchik MJ, Garrett-Sinha LA. Requirement for transcription factor Ets1 in B cell tolerance to self-antigens. J Immunol 2015;195:3574–83.
56. Ramirez K, Chandler KJ, Spaulding C, Zandi S, Sigvardsson M, Graves BJ, et al. Gene deregulation and chronic activation in natural killer cells deficient in the transcription factor ETS1. Immunity 2012;36:921–32.
57. Walunas TL, Wang B, Wang CR, Leiden JM. Cutting edge: the Ets1 transcription factor is required for the development of NK T cells in mice. J Immunol 2000;164:2857–60.
58. Eyquem S, Chemin K, Fasseu M, Chopin M, Sigaux F, Cumano A, et al. The development of early and mature B cells is impaired in mice deficient for the Ets-1 transcription factor. Eur J Immunol 2004;34:3187–96.
59. Mouly E, Chemin K, Nguyen HV, Chopin M, Mesnard L, Leite-de-Moraes M, et al. The Ets-1 transcription factor controls the development and function of natural regulatory T cells. J Exp Med 2010;207:2113–25.
60. Dittmer J. The role of the transcription factor Ets1 in carcinoma. Semin Cancer Biol 2015;35:20–38.
61. el Marjou F, Janssen KP, Chang BH, Li M, Hindie V, Chan L, et al. Tissue-specific and inducible Cre-mediated recombination in the gut epithelium. Genesis 2004;39:186–93.
62. Chiang MY, Xu L, Shestova O, Histen G, L'Heureux S, Romany C, et al. Leukemia-associated NOTCH1 alleles are weak tumor initiators but accelerate K-ras-initiated leukemia. J Clin Invest 2008;118:14.
63. Rakowski LA, Garagiola DD, Li CM, Decker M, Caruso S, Jones M, et al. Convergence of the ZMIZ1 and NOTCH1 pathways at C-MYC in acute T lymphoblastic leukemias. Cancer Res 2013;73:930–41.
64. Ryan RJ, Drier Y, Whitton H, Cotton MJ, Kaur J, Issner R, et al. Detection of enhancer-associated rearrangements reveals mechanisms of oncogene dysregulation in B-cell lymphoma. Cancer Discov 2015;5:1058–71.
65. Kloetgen A, Thandapani P, Ntziachristos P, Ghebrechristos Y, Nomikou S, Lazaris C, et al. Three-dimensional chromatin landscapes in T cell acute lymphoblastic leukemia. Nat Genet 2020;52:388–400.